CORRELATION STUDIES OF PRESSURE FLUCTUATIONS

ON THE GROUND BENEATH A TURBULENT BOUNDARY LAYER

by
Joseph Tant Priestley

Thesis submitted to the Faculty of the Graduate School
of the University of Maryland in partial fulfillment
of the requirements for the degree of
Master of Science

1965

C. 1

ABSTRACT

Title of Thesis: Correlation Studies of Pressure Fluctuations on the
                   Ground Beneath a Turbulent Boundary Layer.

Joseph T. Priestley, Master of Science, 1965

Thesis directed by: Alan J. Faller, Research Associate Professor

Narrow-band pressure correlation measurements in the frequency range

.008 to 1 Hz(cps) were obtained from a cross spectral analysis between

pairs of microphones placed on level ground beneath the wind stream.

The measurements were made over a range of wind speeds from 2.1 to

7.2 meters per second and a range of hemispheric solar radiation con-

ditions varying from 0 to 44 Langleys per hour. Plausibility arguments

are presented which predict for the narrow-band longitudinal and

lateral correlation coefficients: $R_\omega(\xi,0) = e^{-\alpha\xi}\cos(k\xi)$ and $R_\omega(0,\eta) =$

$e^{-\beta\eta}$ where ξ and η are the longitudinal and lateral separations, re-

spectively, and α, β, and k are determined by the experiment. Contrary

to similarity considerations α and k were found not to be strictly

proportional, but rather $\alpha = 0.41k^{1.28}$, α and k being expressed in

$(\text{meters})^{-1}$, over a range $2 < (1/\alpha) < 500$ meters. The relation between

α and β was found to be: $\beta = 1.2\alpha^{.74}$, α and β expressed in $(\text{meters})^{-1}$,

over a range $3 < (1/\alpha) < 500$ meters. For an arbitrary angle with

respect to wind direction evidence is presented which indicates that

$R_\omega(\xi,\eta)$ is very slightly larger than the product $R_\omega(\xi,0)R_\omega(0,\eta)$. A

small amount of data taken relating the convection velocity versus

wavelength to anemometer readings indicates the possibility of predict-

ing the wind profile from pressure fluctuations on the ground.

ACKNOWLEDGMENTS

TABLE OF CONTENTS

LIST OF TABLES

LIST OF FIGURES

SECTION I

INTRODUCTION

This paper reports the results of an investigation into certain statistical properties of the turbulent boundary layer that comes into existence whenever there is sufficiently rapid relative motion between a fluid and a solid body. The random turbulent motions of the fluid cause pressure fluctuations which can be observed at the surface of the solid body.

Historically, the need for the present study grew out of a problem in the infrasonics group at the National Bureau of Standards. This group and others have for more than a decade been interested in monitoring and studying low frequency sound (e.g. less than 1 Hz) in the atmosphere. Because of particularly favorable conditions to propagation of sound within this frequency range, very low absorption and a "channeling" effect (Cook, 1962), infrasonic waves can travel distances of thousands of kilometers. The most serious limitation in detecting these infrasonic waves is background noise caused by turbulent boundary layer pressure fluctuations in the wind stream (see Cook and Young, 1962). Various efforts have been made to reduce this source of background noise (e.g., Daniels, 1959), but greater knowledge of the statistical properties of the turbulent pressure fluctuations is needed.

Boundary layer "wall-pressure" fluctuations are also important in several other fields. These pressure fluctuations acting on ship and submarine sonar transducers diminish the signal-to-noise ratio of received signals. The noise in the cabins of high speed aircraft

1

arises mainly from skin vibration caused by the boundary layer pressure fluctuations (Dyer, 1958). Also structural fatigue in aircraft can be caused by this same vibration.

The specific aim of this study is to gain a quantitative picture of the statistical structure of the boundary layer pressure fluctuations on the ground in the frequency range from one cycle per second to one cycle per minute. To the author's knowledge previous space-time correlation or cross spectral analyses of atmospheric boundary layer pressure fluctuations have not been attempted.

Since the early work of Harrison (1958) and Willmarth (1959) many wind tunnel measurements of this nature have been made; however, many of the results are confusing or at least inconclusive. Much theoretical work has been done by Kraichnan (1956a, 1956b), Lilly and Hodgson (1960), Lilly (1963), Gardner (1963), and White (1964) on the problem of surface pressure fluctuations beneath a turbulent boundary layer; but, generally, the complexity of the mathematics has forced these workers to make idealizations and approximations which many times can be based only upon intuition because of the lack of experimental data.

The purpose of the present study is then twofold: to provide numerical data on atmospheric pressure fluctuations for the workers in this field, and to provide experimental evidence for more general relationships which might be useful to the theoreticians.

SECTION II

FACILITIES AND INSTRUMENTATION

A. Introduction

It was anticipated from the beginning that it would be desirable to first make measurements in a location of flat, easily definable terrain and then, perhaps later, in more complicated terrain. Because of this and other reasons it was decided early in the planning that the equipment should be made as portable as possible. Accordingly, a used one ton panel delivery type truck[1] was obtained and converted into a mobile field station. The completed field station consisted of four pressure transducers, anemometer and wind vane, and the digital and analog recording systems which were mounted in three relay racks in the truck. The system could thus be transported with relative ease, although it did require an ac power line at the site.

B. Location

The experiment was performed at the U.S. Weather Bureau Test and Evaluation Laboratory site near Sterling, Virginia. This site was selected because of the large area of flat terrain and the meteorological support available. The site proper is approximately one and a half miles long in the east-west direction and one half mile north

---

[1] It was perhaps unfortunate that a truck in better condition could not be procured, because much time was wasted attempting to stop up cracks and make the body water proof and mouse proof. On one occasion after the field mice learned to come in through the cracks, they built a nest using for material the data paper as it was fed out of the strip chart recorders.

to south. It is located just beyond the northwest edge of Dulles International Airport. Most of the area has a closely mowed (approximately three inches high) grass cover, although there are trees around part of the perimeter.

The reference point of the experiment (hereafter called base 1) had an upwind fetch of 300 to 400 meters, depending upon the exact wind direction, of very level mowed grass. Beyond this was a strip of small trees and undergrowth ten to twenty feet high. About 90 meters to the southwest was a 15 meter meteorological tower. The mobile field station was located 15 meters southeast of base 1. The wind was from the northwest quadrant for all of the experimental runs.

C. Transducers

The pressure transducers or microphones are a modification of a design that was developed by the National Bureau of Standards. As presently used a transducer consists of a capsule, an electronic oscillator, and a transducer can. The capsule employs a thin metal diaphragm and a fixed backing plate to form a pressure sensitive capacitor. The oscillator which fits on top of the capsule puts out an FM (frequency modulated) electrical signal whose frequency varies almost linearly[2] with pressure on the capsule diaphragm. The nominal center frequency of the FM "tone" is 1550 Hz with a maximum linear swing of 250 Hz either side of center.

The transducer can is a stainless steel container with a backing volume and a forevolume permanently built into it. Both of these volumes are surrounded with two inches of thermal insulation. Figure

---

[2]For the pressures involved in the study, the nonlinearities were not of significance.

la shows a schematic diagram of the microphone assembly while Fig. lb shows the equivalent electrical circuit. The component values given in the figure represents the average values over the four microphones in the high frequency band pass configuration. The low band pass configuration is identical, except that the value of R_2 is increased by a factor of approximately four. The function of the components is as follows: The series combination of C_1 and C_2 with the resistor R_1 forms a 6 dB per octave high pass filter with a 3 dB point at about 1 Hz. The resistor R_2 with forevolume C_3 form a 6 dB per octave low pass filter with a 3 dB point at about 0.5 Hz (0.12 Hz for the low band pass system). Figure 2 shows the average response of the four microphones in both the high and low pass band configurations.[3] The 6 dB per octave high pass filter, which is active throughout most of the band, is needed to complement the frequency spectrum of the turbulent pressure fluctuations. The low pass filter, which is active only at the edge of the pass band, is used to attenuate high frequencies beyond the pass band so as to reduce aliasing caused by the sampling process.

The backing volumes C_1 and forevolumes C_3 are stainless steel containers of approximately one and five gallons capacity respectively. They are filled with stainless steel wool to insure that they operate isothermally over the entire frequency range. The resistors were made by machining small axial holes in cylinders of brass approximately one inch long. The machining had to be done very carefully because the resistance varies with the fourth power of the radius.

---

[3]The response curves shown in Fig. 2 are corrected for the effect of averaging the pressure over the sampling interval.

Because of the cross spectral analyses that were to be performed, the phase characteristics of the microphones had to be matched very closely. The volumes were matched to within about 2% and the resistors could be machined to within about 1%. The capacitances of the capsules turned out to be very difficult[4] to match, but after much trouble, four capsules were obtained which had capacitances that fell within about 4% of the mean. To partially compensate for this mismatch, the resistors R_1 were trimmed such that the measured 3 dB point of the C_1, C_2, and R_1 combination fell within 2% for all four microphones. It was impractical to reduce this error further because of stability problems.

Each completed microphone consisted of a transducer can (25 inches high by 17 inches in diameter) with the pressure inlet, an outdoor type water faucet, mounted on the side. To keep from distrubing the wind flow with the relatively large transducer cans, a fifty foot garden hose was attached to each inlet so that the "microphone openings" were effectively the ends of the garden hoses.

D. Data Recording System

One of the very important initial decisions that had to be made was whether the prime data recording system would be digital or analog. Some criteria that were considered important in making the choice were dynamic range, accuracy, versatility, and cost. The dynamic range and

---

[4]Matching capsules proved to be one of the most difficult parts of the whole experiment. After much effort was expended to find four capsules with matched sensitivities, the capacitances were checked and found to vary over a 50% range. After about three months of futile effort trying to match both capacitance and sensitivity, twelve new capsules were manufactured under very closely controlled conditions and the best four of these were chosen.

accuracy of a digital system is determined solely by the number of bits per data point; i.e., they can be set at any desired level. By contrast the dynamic range of an analog tape recording is about 40 dB for the FM mode and possibly as high as 60 dB for the direct mode, although 50 to 55 dB is more typical under operational conditions. The accuracy of an analog recorder is typically about 1 or 2 percent of full scale. The versatility of the two systems might be about equal if the recording systems alone was considered; however, a digital recording could be taken directly to a general purpose digital computer, whereas an analog record would have to be analyzed on an analog computer designed specifically for the particular computation desired. Thus changing the analysis in the digital system means only a change in program while in the analog system it could mean rebuilding the analog computer. The cost of the two systems would probably be about equal if one included the cost of the analog computer in with the analog system. Because of the above reasons the digital system was chosen.

The following parameters were chosen for the recording system: In order to achieve a wide dynamic range, each data point is represented by a 12 bit binary number. This gives a dynamic range of 72 dB based upon the ratio of the maximum count to the least count. The sampling rate could be changed easily, but in the present experiment the sampling rate f_s[5] was 4 Hz for the high pass band and 1 Hz for the low frequency pass band.

The system, in brief, takes the FM tone from each of the four microphones, counts these tones with electronic counters for the sample time interval of almost $1/f_s$, and then "prints" these four numbers on

_____

[5]Symbols are defined in Appendix A.

the magnetic tape. This process is repeated f_s times per second to produce a magnetic tape with a series of numbers corresponding to the "instantaneous" pressures at each of the four microphones.

Looking at the system in more detail (see Fig. 3) the FM tones from the microphones go through frequency multipliers to increase the resolution to the point of taking full advantage of the 12 bit recording system. The signals out of the four frequency multipliers are each sent to one of the four counters.

The 12 bit recording system has a resolution of one part in 2^{12} or one part in 4096. The total frequency swing of the FM tone from a microphone is ±250 or 500 Hz. Therefore, if this signal went directly to a counter and were counted for one second, the resolution would be only one part in 500. By first multiplying this frequency by eight we obtain a resolution of one part in 4000, making full use of the resolving capability of the 12 bit recording system. When 1/4 second sampling time is used the multiplication factor is changed to 32.

The sequence of events in one recording cycle is the following: The counters count the frequency multiplied FM signals from the microphones for 1 second (or 1/4 second); then a pulse arrives from the clock and stops the counters. The numbers in the four counters are then "dumped" into a shift register, the counters are set to zero, and the counting is restarted. The total "dead" time of the counters is 40 μs, a small fraction of the 1 second (or 1/4 second) sampling time. While the counters are again counting, the shift register shifts the characters[6] out one by one and they are recorded onto the magnetic

---

[6]A character is six bits of data. It thus requires two characters for each 12 bit data point.

tape. For each recording cycle 12 characters (one data block)[7] are recorded onto the tape. One data block consists of eight characters from the microphone counters, two characters from the anemometer counter, one character from the seconds register in the clock, and a one character flag.[8] The data goes onto the magnetic tape in standard computer format with parity check bits. At the end of every 2,400 data blocks[9] the system records the time in hours and minutes and then inserts an inter-record gap.[10] An end-of-file gap can be inserted any place in the tape by pressing a button.

The entire digital recording system is built in modular form. The frequency multiplier module which contains all four multipliers was designed for this project. Each multiplier is made up of five stages of frequency doubling. The development of some rather unique circuitry allows the frequency multiplier to operate over a wide range of input frequencies. The counters which were also designed for this project use rather conventional digital circuitry. The shift register and control module were standard modules which had been developed by the Measurement Automation Section of the National

---

[7] A data block, being made up of 12 six bit characters, thus contains 72 bits; i.e. two IBM words.

[8] The seconds character and the flag that are recorded in every data block are checked in the computer to make sure the recording system was working properly.

[9] At the sampling rates of 1/4 second and 1 second the 2,400 data blocks represent 10 minutes and 40 minutes, respectively, of recording time.

[10] The operation of recording the time and inserting the inter-record gap is accomplished without the loss of data. This makes it possible to analyze two or more records of data as a single run.

Bureau of Standard. The electronic clock and the stepping tape recorder were purchased commercially.

The analog recording system for the microphones consisted of frequency-to-voltage converters and strip-chart recorders. These records are used chiefly for visually monitoring the microphone signals during recording. Strip-chart recorders were also used for recording the anemometer and wind vane data.

SECTION III

EXPERIMENTAL PROCEDURE

A. Introduction

A reference point (base 1) was chosen which had a large unob-
structed fetch for the most prevalent wind direction. The truck was
then parked downwind from base 1 and connected to the power line. A
surveyor's transit was used to position stakes thirty meters from base
1 at the north, south, and west compass points and also at 15 degree
intervals in the northwest quadrant. The anemometer and wind vane
were mounted at a height of 4.27 meters on a mast attached to the
truck. The truck was 15 meters southeast of base 1. Ninety meters
southwest of base 1, a Weather Bureau anemometer and wind vane were
mounted at a height of 10 meters on a tower.

B. Microphone Positions

The experimental procedure, in brief, consists of positioning the
microphones according to a prearranged pattern relative to the wind
direction and recording data. Actually, the transducer cans themselves
are not placed in the "microphone positions", but rather fifty foot
garden hoses are connected to the transducer can inlets and the other
ends of the hoses are placed at the microphone positions. The trans-
ducer cans are placed downstream or to the side, well away from the
microphone positions so as not to interfere with the normal flow past
these positions. The ends of the hoses at the microphone positions are
placed well within the grass so as to detect only the static pressure

11

fluctuations.[11]

In order to simplify the data reduction, a small number of micro-phone arrangements was standardized. The two basic patterns were the linear array and the square array. Since the meteorological conditions would not be expected to be exactly reproducible between runs, it was important to obtain data representing as many different separations as possible for each individual run. This was particularly true for the linear array when the functional form of the correlation coefficient versus separation was being explored. Since the system included four microphones, six combinations of pairs were possible.

For a linear array, the widest range of spacings can be obtained if the microphone separations form a logarithmic sequence. Since it is not possible to have the spacings form an exact logarithmic sequence using all six combinations, the following approximations were standardized.

For a small array microphone position co-ordinates of 0, 1.5, 2.5, and 6.5 meters were chosen. This provided separations of 1, 1.5, 2.5, 4, 5, and 6.5 meters. In addition to this, a larger linear array was also used. The position co-ordinates of this array were 0, 9.75, 16.25, and 45.45 meters giving separations of 6.5, 9.75, 16.25, 29.2, 35.7, and 45.45 meters.[12] Table 1 lists the above microphone spacings as

---

[11] In order to verify that only the static pressure fluctuations were detected, the hose ends from two microphones were placed at right angles together in the grass; one end facing into the wind direction and one perpendicular to the wind direction. The strip-chart record-ings of the two microphone outputs were superimposed on a "light box" and found to agree typically within the width of the trace, a fraction of a percent.

[12] It was initially intended that the large microphone spacings be a simple scale-up of the small spacings; however, in the hurry to set up the large array the first time, the scaling was miscalculated.

small and large, respectively. Several sizes of square arrays were also used, but only the 9.15 and the 6.10 meter arrays will be reported on here because the wind speed was so low on the others that there was considerable acoustical background interference.

C. Data Recording

On windy days the wind instrument strip-chart records were visually monitored. During periods when the wind speed and direction tended to maintain a constant average, the microphones would be set up according to one of the prearranged patterns. A steel tape would be anchored at base 1 and extended in the desired direction. One microphone (hose end) would be placed at base 1 and the others would be placed at the prescribed distances along the tape line. The tape would then be removed and taken back to the truck. The digital recording system would be turned on and an end-of-file mark would be inserted. The time, the file number, and a description of the microphone array along with other recording parameters would be recorded in the log book. Usually, several hours of data would be recorded continuously in hopes of getting data during an interval of steady wind in the right direction.

D. Data Selecting

After a reel of magnetic tape had been recorded, the wind instrument strip-chart records would be scrutinized. The average wind speed and direction along with an estimate of the standard deviation of each of these (one sixth of the peak-to-peak excursion) would be tabulated. From this tabulation, the most promising looking runs would be selected.

The attempt was made to use only those records in which the average wind direction was within 3° of the desired direction. From other

indications, however, it turned out that, typically, the average wind direction was 5 to 8 degrees different from the nominal. This error was possibly due to deflection of the airflow past the wind vane because of interference with the truck body. For the linear arrays this error was not considered serious, however, for the square arrays a correction was made.[13]

A short initial computer program was written which would select the desired runs by file number and clock time. These records would then be checked for parity error, the proper number of words, and for flags at the right locations. The data would then be rerecorded in a format suitable for input to the program described in Appendix B.

---

[13]This is discussed more fully in SECTION V D.

SECTION IV

MATHEMATICAL CONSIDERATIONS

A. Relationship Between Narrow Band Correlation and Cross Spectral Density[14]

Let $p(x,y,t)$ be the fluctuating static pressure at time t at a point (x,y) on the surface under consideration. The pressure field will be considered to be statistically stationary and spatially homogeneous over the surface. The mean value of $p(x,y,t)$ is zero. On this basis the two point pressure covariance, which is the mean value of the product $p(x,y,t)\,p(x+\xi,y+\eta,t+\tau)$, is a function of the space and time increments only, and we denote it by

$$P(\xi,\eta,\tau) = <p(x,y,t)\,p(x+\xi,y+\eta,t+\tau)> \qquad (4.1)$$

where the brackets $< >$ indicate a large scale space or time average.

The space-time covariance $P(\xi,\eta,\tau)$ can be associated with a frequency spectrum, the relation between the two being given by the Fourier transform pair

$$P(\xi,\eta,\tau) = \int_{-\infty}^{\infty} K(\xi,\eta,\omega)\,e^{i\omega\tau}d\omega$$

$$K(\xi,\eta,\omega) = \frac{1}{2\pi}\int_{-\infty}^{\infty} P(\xi,\eta,\tau)\,e^{-i\omega\tau}d\tau . \qquad (4.2)$$

$K(\xi,\eta,\omega)$ will, in general, be a complex quantity with real and imaginary parts $Co(\xi,\eta,\omega)$ and $Q(\xi,\eta,\omega)$ which are, respectively, even and odd functions of ω. $K(\xi,\eta,\omega)$ is referred to as the cross-spectral density

---

[14]The derivation in this subsection, except for notation and other slight changes, is that given by Bull (1963).

of the fluctuating pressure; while $Co(\xi,\eta,\omega)$ and $Q(\xi,\eta,\omega)$ are referred to as the co-spectrum and quadrature spectrum respectively. In the particular case $\xi=\eta=0$ the cross-spectral density $K(\xi,\eta,\omega)$ becomes the "power" spectral density $\varphi(\omega)$.

If the pressure signal $p(x,y,t)$ is passed through a filter (a linear, constant parameter system) whose impulse response function is $h(t)$ and frequency response function is

$$Y(i\omega)= \int_{o}^{\infty}h(\gamma)e^{-i\omega\gamma}d\gamma \qquad (4.3)$$

the filtered signal will be

$$q(x,y,t)= \int_{o}^{\infty}h(\gamma)p(x,y,t-\gamma)d\gamma. \qquad (4.4)$$

The product of filtered signals from two points will therefore be

$$q(x,y,t)q(x+\xi,y+\eta,t+\tau)= \int_{o}^{\infty}h_1(\mu)p(x,y,t-\mu)d\mu \int_{o}^{\infty}h_2(\nu)p(x+\xi,y+\eta,t+\tau-\nu)d\nu$$

$$= \int_{o}^{\infty}\int_{o}^{\infty}h_1(\mu)h_2(\nu)p(x,y,t-\mu)p(x+\xi,y+\eta,t+\tau-\nu)d\mu d\nu$$

Taking averages and assuming that the operations of averaging and integration may be interchanged we obtain,

$$<q(x,y,t)q(x+\xi,y+\eta,t+\tau)>$$

$$=\int_{o}^{\infty}\int_{o}^{\infty}h_1(\mu)h_2(\nu)<p(x,y,t)p(x+\xi,y+\eta,t+\tau-\nu)>d\mu d\nu$$

$$=\int_{o}^{\infty}\int_{o}^{\infty}h_1(\mu)h_2(\nu)P(\xi,\eta,\tau+\mu-\nu)d\mu d\nu$$

$$=\int_{o}^{\infty}\int_{o}^{\infty}h_1(\mu)h_2(\nu)\int_{-\infty}^{\infty}K(\xi,\eta,\omega)e^{i\omega(\tau+\mu-\nu)}d\omega d\mu d\nu$$

$$=\int_{-\infty}^{\infty}K(\xi,\eta,\omega)e^{i\omega\tau}\int_{o}^{\infty}h_1(\mu)e^{i\omega\mu}d\mu \int_{o}^{\infty}h_2(\nu)e^{-i\omega\nu}d\nu d\omega$$

$$\int_{-\infty}^{\infty}Y_1^{*}(i\omega)Y_2(i\omega)K(\xi,\eta,\omega)e^{i\omega\tau}d\omega \qquad (4.5)$$

where $Y_1^*(i\omega)$ is the complex conjugate of $Y_1(i\omega)$. If the two filters have identical characteristics then

$$<q(x,y,t)q(x+\xi,y+\eta,t+\tau)> = \int_{-\infty}^{\infty} |Y(i\omega)|^2 K(\xi,\eta,\omega)e^{i\omega\tau}d\omega. \qquad (4.6)$$

Now suppose that the frequency response of the filters is given by

$$|Y(i\omega)|^2 = \begin{cases} 1 & \text{for } (\omega_0-\Delta\omega/2) < |\omega| < (\omega_0+\Delta\omega/2) \\ 0 & \text{otherwise.} \end{cases} \qquad (4.7)$$

That is, we consider band pass filters with rectangular response characteristics centered at ω_0 and with bandwidth $\Delta\omega$, which we shall here assume to be small. Also, since the fluctuating pressure has been considered as a stationary random variable, the filtered signals will be stationary random variables, and, hence, the mean value of Eq. (4.6), as indicated by the right hand side of the equation, is independent of x,y, and t; for filters described by Eq. (4.7), it will be denoted by $P(\xi,\eta,\tau;\omega_0)$. Thus in this case

$$<q(x,y,t)q(x+\xi,y+\eta,t+\tau)>=P(\xi,\eta,\tau;\omega_0) \qquad (4.8)$$

$$=[K(\xi,\eta,\omega_0)\exp(i\omega_0\tau)+K(\xi,\eta,-\omega_0)\exp(-i\omega_0\tau)]\Delta\omega$$

In view of the fact that $Co(\xi,\eta,\omega)$ and $Q(\xi,\eta,\omega)$ are respectively even and odd functions of ω, Eq. (4.8) reduces to

$$P(\xi,\eta,\tau;\omega)=2[Co(\xi,\eta,\omega)\cos\omega\tau-Q(\xi,\eta,\omega)\sin\omega\tau]\Delta\omega \qquad (4.9)$$

where the suffix on ω_0 has now been dropped.

The correlation given by Eq. (4.9) may be normalized by dividing it by $P(0,0,0;\omega)$ to give

$$R_\omega(\xi,\eta,\tau) = \frac{P(\xi,\eta,\tau;\omega)}{P(0,0,0;\omega)}$$

$$= \frac{Co(\xi,\eta,\omega)\cos\omega\tau-Q(\xi,\eta,\omega)\sin\omega\tau}{Co(0,0,\omega)} \qquad (4.10)$$

$$= \left|\frac{K(\xi,\eta,\omega)}{\varphi(\omega)}\right| \cos(\omega\tau+\theta)$$

where $\theta=\tan^{-1}\dfrac{Q(\xi,\eta,\omega)}{Co(\xi,\eta,\omega)}$. $R_\omega(\xi,\eta,\tau)$ is called the narrow band correlation coefficient.

B. A Modified Taylor's Hypothesis

In order to proceed further, let us consider some of the experimentally established characteristics of turbulence. Taylor's hypothesis (Lumley and Panofsky, 1964, p. 56) states that if the turbulent velocity fluctuations are small compared with the mean stream velocity, the time variations in the velocity, as observed at a fixed point in the flow, would be approximately the same as that due to the convection of an unchanging spatial pattern past the point with the mean flow velocity U; i.e. $u(t)_{x=o}=u\left(\dfrac{-x}{U}\right)_{t=o}$ where x represents position measured in the mean flow direction. Lin (1952) pointed out that Taylor's hypothesis is valid only if the turbulence level is low, viscous forces are negligible, and the mean shear is small. When applied to surface pressure variations under a turbulent boundary layer, the first two conditions are probably fairly well met, but the third is at least questionable. Despite this, it is not uncommon practice to apply Taylor's hypothesis to surface pressure fluctuations (Willmarth, 1959; Bull, 1963). In the present work we shall use a "modified Taylor's hypothesis" which will allow the convection velocity of disturbances U_c to be a function of frequency.[15] This will to a large degree overcome the requirement that the mean shear be small.

Let us now look back at Eq. (4.10). The correlation coefficient $R_\omega(\xi,\eta,\tau)$ represents a comparison between two narrow band (almost sinusoidal) signals. The expression $(\omega\tau+\theta)$ represents the average

---

[15]Wills (1963) gives an excellent discussion on convection velocity.

phase difference between the two signals. In particular, $\omega\tau$ represents the phase difference due to relative time variation and θ represents the phase difference due to relative spatial variation. Under the assumption of the modified Taylor's hypothesis we have $\theta = -\dfrac{\omega\xi}{U_c}$ where ξ measures separation in the flow direction. Thus

$$R_\omega(\xi,\eta,\tau) = \left|\frac{K(\xi,\eta,\omega)}{\varphi(\omega)}\right| \cos\left(\omega\tau - \frac{\omega\xi}{U_c}\right). \qquad (4.11)$$

Also of importance is the concept of coherence which is defined:

$$Coh(\xi,\eta,\omega) = \frac{Co^2(\xi,\eta,\omega) + Q^2(\xi,\eta,\omega)}{\varphi^2(\omega)}.$$

We notice that:

$$Coh^{1/2}(\xi,\eta,\omega) = \left|\frac{K(\xi,\eta,\omega)}{\varphi(\omega)}\right| \; ;$$

therefore,

$$R_\omega(\xi,\eta,\tau) = Coh^{1/2}(\xi,\eta,\omega) \cos\left(\omega\tau - \frac{\omega\xi}{U_c}\right). \qquad (4.12)$$

Two other forms of Eq. (4.12) will be of particular interest to us. If we optimize the correlation coefficient with respect to time delay, i.e. set $\omega\tau = \dfrac{\omega\xi}{U_c}$ we obtain:

$$R_{opt,\omega}(\xi,\eta) = R_\omega(\xi,\eta,\tau_{opt}) = Coh^{1/2}(\xi,\eta,\omega). \qquad (4.13)$$

Also of interest is the narrow band space correlation coefficient, i.e. for $\tau=0$. Thus

$$R_\omega(\xi,\eta,0) = Coh^{1/2}(\xi,\eta,\omega) \cos\left(\frac{\omega\xi}{U_c}\right). \qquad (4.14)$$

SECTION V

CORRELATION COEFFICIENT

A. Introduction

The computer program which was used for the cross-spectral and power spectral analyses is described briefly in Appendix B. The maximum number of lags used was 120 for all runs. The number of data points per microphone was either 2400 or 4800 depending upon whether the run number ended in one letter or two letters, respectively (see Table 1). The computer output of the analysis of a pair of channels is a tabular print-out which includes the spectral densities of both channels, the co-spectral density, and the quadrature spectral density versus the frequency; i.e. ϕ_1, ϕ_2, Co, and Q versus f. The frequencies (in Hz) range from $1/(2T_L)$ to $f_s/2$ in intervals of $1/(2T_L)$ where T_L is the maximum time lag in the cross and auto-correlations, and f_s is the sampling rate of the raw data. This gives a total number of frenquencies equal to the maximum number of lags; i.e. 120.

It was considered much more useful to have the spectral data referred to a logarithemic (constant percentage bandwidth) rather than a linear frequency scale. Accordingly, the frequencies from the computer output were arranged into groups representing 1/3-octave band-widths (see Tables 2 and 3) and the corresponding values of the spectral densities — ϕ_1, ϕ_2, Co, and Q — were averaged within each group. This procedure had the desirable effect of decreasing the statistical fluctuation of the data in the high frequency region while also reducing the quantity of data.

20

There is, of course, the danger of obscuring relevant features of the data by taking too wide a bandwidth. It has been pointed out by Wills (1963) and Bull (1963) that if $R_\omega^{(m)}(\xi,\eta)$ is the measured correlation coefficient and $R_\omega(\xi,\eta)$ the actual correlation coefficient, we have

$$\frac{R^{(m)}(\xi,\eta)}{R_\omega(\xi,\eta)} = \frac{\sin\left(\frac{1}{2}\frac{\Delta\omega}{\omega}\frac{\omega\xi}{U_c}\right)}{\frac{1}{2}\frac{\Delta\omega}{\omega}\frac{\omega\xi}{U_c}} \tag{5.1}$$

where $\Delta\omega/\omega$ is the fractional bandwidth and $\omega\xi/U_c$ is the normalized separation. At a separation of zero, this causes no error. At separations of $\omega\xi/U_c = \pi$ and 2π, the succeeding minimum and maximum in the correlation coefficient curve, Eq. (5.1) gives values of .98 and .92, respectively. Typically at distances of $\omega\xi/U_c = \pi$ and 2π, the correlation coefficient is not greater than 0.6 and 0.3, respectively; therefore, the error caused by the 1/3-octave band width is considered negligible.

For each run, the quantities $Coh^{1/2}(\xi,\eta,\omega)$ and $R(\xi,\eta)$ for each pair of microphones were computed at each 1/3-octave band according to the relations

$$Coh(\xi,\eta,\omega) = \frac{Co^2(\xi,\eta,\omega) + Q^2(\xi,\eta,\omega)}{\phi_1(\omega)\,\phi_2(\omega).}$$

and

$$R_\omega^2(\xi,\eta) = \frac{Co^2(\xi,\eta,\omega)}{\phi_1(\omega)\,\phi_2(\omega)}$$

B. Logitudinal Correlation Coefficient

1. <u>Experimental data</u>. The longitudinal data consists of seven runs in which a linear microphone array was oriented parallel to the nominal average wind direction (marked "||" in Table 1). These runs, as shown

in Table 1, cover a range of wind speeds from 2.1 to 7.2 meters/sec (as measured by the anemometer at 4.27 meters). While not measured explicitly, an indication of the range in atmospheric stability can be deduced from the hemispheric radiation and the relative cloud cover.

For each of the seven runs, the values of $Coh^{1/2}(\xi,0,\omega)$ and $R_\omega(\xi,0)$ versus separation ξ were plotted, a separate graph being made for each value of ω. Figures 4a and 4p show these data plotted for a typical run. The plots of $R_\omega(\xi,0)$, particularly the latter half, clearly exhibit the cosine nature of the function as derived in Eq. (4.14).

$$R_\omega(\xi,0) = Coh^{1/2}(\xi,0,\omega)\cos\left(\frac{\omega}{U_c}\xi\right) \qquad (4.14)$$

It is also evident from the data that the value of $Coh^{1/2}(\xi,0,\omega)$ tends to form an "envelope" or a maximum amplitude for the values of $R_\omega(\xi,0)$.

Empirically, an exponential curve fits the $Coh^{1/2}(\xi,0,\omega)$ data well within experimental error. The product of the above exponential curve with a suitable cosine curve is an equally good fit to the $R_\omega(\xi,0)$ data. The curve used to fit the $Coh^{1/2}(\xi,0,\omega)$ data is $e^{-\alpha\xi}$ where α is chosen according to the best least squares fit. Using the above α, a value of k was found which gave the curve $e^{-\alpha\xi}\cos(k\xi)$ versus ξ the best least squares fit to the $R_\omega(\xi,0)$ data. This provided a value for α and for k corresponding to each of the center frequencies of the 1/3-octave bands. Figures 4a to 4p are typical of the degree to which these functional forms fit the experimental data.

2. _Discussion._ Several investigators have measured the longitudinal correlation coefficient in narrow frequency bands. Harrison (1958), Bull, et al. (1963)[16] and Corcos (1964) find that the

_____

[16]Bull, et al. (1963) divides the spectrum into two parts and finds that for the high frequencies $R_\omega(\xi,0,0)=A(\omega\xi/U_c)\cos(\omega\xi/U_c)$ but for the low frequencies A is independent of ω.

correlation coefficient can be expressed in the following form:

$$R_\omega(\xi,0,0) = A\left(\frac{\omega\xi}{U_c}\right) \cos\frac{\omega\xi}{U_c} . \tag{5.4}$$

Likewise, Willmarth and Wooldridge (1962) find that the optimized correlation coefficient may be expressed in the form

$$R_{opt,\omega}(\xi,0) = A\left(\frac{\omega\xi}{U_c}\right) \tag{5.5}$$

In all of the above works except Harrison (1958), the curve $A(\omega\xi/U_c)$ looks very much like an exponential decay, however, save for Bull, et al. (1963), none of the references give an analytic expression. They just present the data with a smooth curve drawn through it. Bull, et al. gives the expression

$$A\left(\frac{\omega\xi}{U_c}\right) = e^{-0.1 \ \omega\xi/U_c} \tag{5.6}$$

for frequencies greater than $\omega\delta*/U_c = 0.36$.

Bakewell, et al. (1962) made measurements in one-octave bands and gives the results

$$R_f(\xi,0,0) = e^{-2(f\xi/U_c)^2} \cos\frac{2\pi f\xi}{U_c} . \tag{5.7}$$

The rapid decay with respect to $f\xi/U_c$ seems to be an artifact of using too wide a bandwidth. In later measurements with narrower filters (Bakewell, 1963; Bakewell, 1964), he presents the results

$$R_f(\xi,0,0) = \exp(-0.7 \ f\xi/U_c)\cos\frac{2\pi f\xi}{U_c} \tag{5.8}$$

In review, the consensus among the experimenters is that the correlation coefficient may be expressed in the general form

$$R_\omega(\xi,0) = A\left(\frac{\omega\xi}{U_c}\right) \cos\frac{\omega\xi}{U_c} . \tag{5.9}$$

While most workers give $A\left(\frac{\omega\xi}{U_c}\right)$ only in the form of a graph, a few give it explicitly in terms of an exponential function.

Among both theorists and experimenters there seems to be little

controversy that the narrow band longitudinal correlation coefficient

can be expressed in the form

$$R_\omega(\xi,0)=R_{opt,\omega}(\xi,0)\cos\frac{\omega\xi}{U_c} \ . \tag{5.10}$$

It is understood that $R_{opt,\omega}(\xi,0)$ must equal one at $\xi=0$, and it is

generally agreed that it asymptotically approaches zero as ξ increases,

but beyond this point difficulties arise.

Taylor (1922) and Hinze (1959, p.35) give very general arguments

which indicate that the slope of $A_\omega(\xi)$ should be zero at $\xi=0$.[17] While

the arguments themselves seem quite rigorous, historically the data

have not generally substantiated this point.[18] It must be admitted, of

course, that to measure the cross correlation as a function of separa-

tion as the separation approaches zero, requires vanishing small trans-

ducers. Since experimentally this requirement can never be achieved,

the only hope lies in the development of a theory which predicts more of

the curve than just the slope at $\xi=0$.

Apparently the only existing theoretical treatments of turbulent

space-time correlations for surface pressure fluctuations are two

remarkable papers by Gardner (1963) and White (1964), respectively.

White's work uses the basic approach of Gardner, but refines and

extends this work; therefore we shall use only White's results in the

present discussion. White presents the correlation coefficient in the

---

[17]In their original contexts, both of these arguments were applied
to broad-band velocity correlations; however, the assumptions are broad
enough to include wall-pressure correlations.

[18]See Dryden, et al. (1937, p. 10) for an example of turbulent
velocity correlations or Willmarth and Wooldridge (1962) for an example
of wall-pressure correlations.

following form:

$$R_\omega(\xi,0) = A\left(\frac{\omega\xi}{U_c}, \frac{\omega\delta}{U_\infty}\right) \cos\frac{\omega\xi}{U_c} \tag{5.11}$$

where A is a weak function of the boundary layer thickness δ. Since A involves integrals which require numerical evaluation on a computer, White presents the function as a family of curves (see Fig. 5). His paper assumes a one-seventh power law wind profile and the resulting curves for A versus $\omega\xi/U_c$ do have a zero slope at $\xi=0$. In later work,[19] however, he assumed a different wind profile and obtained curves for A which had finite slopes at $\xi=0$. Because of the above rather curious result, the nature of the function $A=R_{opt,\omega}(\xi,0)$, at least in the neighborhood of $\xi=0$, is presently somewhat uncertain.

While the ultimate solution to the problem undoubtedly lies in a good physical theory — probably similar in approach to that of Gardner and White — the fact remains that the present data, and that of other experimenters,[20] can be much more closely represented by an exponential curve. For this reason, the following will be presented, by way of a plausibility argument, to show that it is not unreasonable to expect the function $R_{opt,\omega}(\xi,0) = Coh^{1/2}(\xi,0,\omega)$ to decay exponentially with ξ.

We shall here assume that we have a constant average wind speed and direction blowing across a level horizontal surface. We also assume (as in SECTION IV) that the turbulence in homogeneous in horizontal planes making cross correlations, functions of co-ordinate separations only. The xy plane will be taken as the horizontal surface with the wind in the

---

[19] Telephone conversation with White; June 23, 1965.

[20] See, for example, Serafini (1962, Fig. 27); Bull, et al. (1963, Figs. 53, 54); Willmarth and Wooldridge (1962, Figs. 9, 10).

plus x direction.

Let the fluctuating pressures $p(x,0,t)$ and $p(x+\xi,0,t+\tau)$ pass through identical narrow band filters of the type described by Eq. (4.7). The filtered signals with center frequency ω will be designated $q(x,0,t)$ and $q(x+\xi,0,t+\tau)$ respectively. It is desired to consider the downstream pressure $q(x+\xi,0,t+\tau)$ at a delayed time τ such that its correlation with $q(x,0,t)$ is a maximum. In SECTION IV we learned that the optimum correlation occurred at a time delay of $\tau=\xi/U_c$ where the convection velocity U_c may be a function of ω. Therefore, we examine $q(x+\xi,0,t+\xi/U_c)$.

Let us consider the fluctuating pressures at the points A, B, and C located at $(x,0)$, $(x+\xi,0)$ and $(x+2\xi,0)$ respectively. We stipulate that the time lags τ will always be optimized for maximum correlation with the pressure at point A. Thus we consider

$$q_A = q(x,0,t)$$
$$q_B = q(x+\xi,0,t+\xi/U_c)$$
$$q_C = q(x+2\xi,0,t+2\xi/U_c)$$

(5.12)

Now q_B may be divided into two parts[21]

$$q_B = q_{BA} + q_{BA*}$$

(5.13)

such that q_{BA}[22] is completely correlated with q_A and q_{BA*} is completely uncorrelated with q_A. Additionally we have[23]

[21] See Appendix C.

[22] When more than one subscript is used on q the first one completely specifies the co-ordinates and time.

[23] Since the turbulent pressure field is homogeneous in the xy plane we have $\langle q_A^2 \rangle = \langle q_B^2 \rangle = \langle q_C^2 \rangle$. Therefore, the ratio of the rms values of the pressures as shown in Eq. (C6) is equal to unity.

$$q_{BA} = R_{opt,\omega}(\xi) q_A \, .$$ (5.14)

Let us consider the pressures q_{BA} and q_{BA*}. Since they are both narrow band signals with frequency centered at ω, there is no possible way to distinguish between them without reference to the pressure at an upstream point. We conclude that the coherence of the "energy" represented by each of them must obey the same "decay law" as the coherence of the energy represented by the entire signal q_B. We can now say that q_{BA}, the part of the signal at B which is coherent with q_A, will lose coherence by an additional factor $R_{opt,\omega}(\xi)$ upon traveling the additional distance ξ to the point C. Thus we have

$$q_{CA} = R_{opt,\omega}(\xi) q_{BA}$$ (5.15)

and from eq. (5.8)

$$q_{CA} = R^2_{opt,\omega}(\xi) q_A \, .$$ (5.16)

Now since

$$q_{CA} = R_{opt,\omega}(2\xi) q_A$$ (5.17)

we have the result,

$$R_{opt,\omega}(2\xi) = R^2_{opt,\omega}(\xi) \, .$$ (5.18)

This may be generalized to give

$$R_{opt,\omega}(n\xi) = R^n_{opt,\omega}(\xi)$$ (5.19)

which has the solution

$$R_{opt,\omega}(\xi) = e^{-\alpha\xi}$$

or (5.20)

$$Coh^{\frac{1}{2}}(\xi,0,\omega) = e^{-\alpha\xi} \, .$$

It is understood that α is a function of ω. From Eq. (4.14) the narrow band logitudinal correlation coefficient is

$$R_\omega(\xi,0) = e^{-\alpha\xi} \cos(k\xi)$$ (5.21)

where $k = \dfrac{\omega}{U_c}$.

We notice that α and k are both reciprocal lengths. In particular, $\frac{1}{\alpha}$ measures the coherence scale and $\lambda = \frac{2\pi}{k}$ is the wave length of the disturbance. We could at this point inquire into a possible functional relation between α and k; however, this will be saved for the discussion on relationships between correlation parameters.

C. Lateral Correlation Coefficient

1. <u>Experimental data</u>. The lateral data consists of three runs in which a linear microphone array was oriented perpendicular to the nominal average wind direction (marked $\perp$ in Table 1). For each of the three runs the values of $Coh^{1/2}(0,\eta,\omega)$ and $R_\omega(0,\eta)$ were computed. If we set $\xi=0$ in Eq. (4.14) we obtain

$$R_\omega(0,\eta) = Coh^{1/2}(0,\eta,\omega). \tag{5.22}$$

In the actual data[24] R - as a rule - is slightly smaller than $Coh^{1/2}$, but this can be completely accounted for by slight statistical variations and a few degrees error in wind direction. Since error of one sort or another is the only reason that the measured values of $R_\omega(0,\eta)$ are smaller than the measured values of $Coh^{1/2}(0,\eta,\omega)$, the values of $Coh^{1/2}(0,\eta,\omega)$ are a more reliable estimate of the lateral correlation coefficient than the measured values of correlation coefficient. Henceforth, $Coh^{1/2}(0,\eta,\omega)$ shall be used for lateral correlation coefficient.

The lateral correlation coefficient versus distance could be fitted with the exponential function equally as well as the longitudinal $Coh^{1/2}(\xi,0,\omega)$ data.

---

[24] Actual graphs of $R_\omega(0,\eta)$ and $Coh^{1/2}(0,\eta,\omega)$ will not be presented here because it is felt they would add little compared to the space taken. The degree to which the $Coh^{1/2}(0,\eta,\omega)$ data fit exponential curves is similar to that of the longitudinal data presented in Figs. 4a – 4p.

2. _Discussion_. The state of affairs regarding the lateral correlation coefficient is quite analogous to that of the longitudinal optimized correlation coefficient. Bull, et al. (1963) and Corcos (1964) find that the narrow band lateral correlation coefficient may be expressed in the form

$$R_\omega(0,\eta) = B\left(\frac{\omega\eta}{U_c}\right).$$

(5.23)

Bull, et al. find, in particular, that

$$R_\omega(0,\eta) \approx e^{-.715\omega\eta/U_c}$$

(5.24)

for frequencies greater than $\frac{\omega\delta^*}{U_c} = 0.36$.

On the theoretical side, the arguments of Taylor (1922) and Hinze (1959) should apply to the lateral correlation coefficient equally as well as they do in the longitudinal case. The data, however, (as in the longitudinal case) seem to indicate that the slope of $R_\omega(0,\eta)$ at $\eta=0$ has a value other than zero.

Although there are much less data available in the case of the lateral correlation coefficient, the data that are available can be quite well represented by the exponential function. A plausibility argument, almost identical[25] to that given for the longitudinal correlation coefficient, can be made to justify the exponential form for the lateral correlation coefficient. An argument using those same basic concepts will be presented here in a slightly different form and with an important extention.

We make the same assumptions here regarding horizontal homogeneity and time stationarity that we made in previous sections. This time,

---

[25]The argument for the lateral case is actually simpler because it is not necessary to introduce a time delay to compensate for the spatial phase shift.

however, we choose the three points A, B, and C to be located at the co-ordinate positions $(0,y)$, $(0,y+\epsilon\eta)$ and $(0,y+\eta)$, respectively, where ϵ is a number between zero and one. The pressure signals p, after having passed through narrow band filters will be designated by the symbol q. We thus consider the signals

$$q_A = q(0,y,t)$$

$$q_B = q(0,y+\epsilon\eta,t)$$

$$q_C = q(0,y+\eta,t).$$

(5.25)

Let us agree that under the above conditions and under a fixed set of turbulence parameters, the lateral correlation coefficient is a unique function of η which has the value of unity at $\eta=0$ and decreases monotomically with increasing separation η.

From Appendix G the pressure signal q_B may be divided into two parts such that

(5.26)

$$q_B = q_{BA}+q_{BA*}$$

where q_{BA} is that part of the signal q_B which is completely correlated with q_A and q_{BA*} is completely uncorrelated with q_A. Also we have

(5.27)

$$q_B = R_\omega(0,\epsilon\eta)q_A+q_{BA*}.$$

Since it might be more aesthetically pleasing to deal with average power rather than instantaneous amplitudes, we square and average each side of Eq. (5.27). Thus we have

(5.28)

$$<q_B^2> = R_\omega^2(0,\epsilon\eta)<q_A^2> + <q_{BA*}^2>.$$

Notice the cross term on the right goes out because it is the covariance between two uncorrelated signals. The signal at point C is,

(5.29)

$$q_C = R_\omega(0,\{1-\epsilon\}\eta)q_B+q_{CB*}$$

and the "power" at C is,

$$<q_B^2> = R_\omega^2(0,\{1-\epsilon\}\eta)<q_B^2> + <q_{CB*}^2>. \qquad (5.30)$$

Substituting Eq. (5.28) into (5.30) we obtain

$$<q_C^2> = R_\omega^2(0,\{1-\epsilon\}\eta)R_\omega^2(0,\epsilon\eta)<q_A^2> + R_\omega^2(0,\{1-\epsilon\}\eta)<q_{BA*}^2> + <q_{CB*}^2> \qquad (5.31)$$

Now we may ask: what is the power $<q_{CA}^2>$, that part of the power $<q_C^2>$ which is completely correlated with the signal q_A. The term on the right containing $<q_{BA*}^2>$ is by hypothesis uncorrelated with q_A; therefore, it goes out. The term $<q_{CB*}^2>$ has zero correlation with the signal at B, therefore, it would also be expected to have zero correlation with the signal at the more distant point A.[26] Therefore, we have

$$<q_{CA}^2> = R_\omega^2(0,\{1-\epsilon\}\eta)R_\omega^2(0,\epsilon\eta)<q_A^2>. \qquad (5.32)$$

Considering only the points A and C we also have the relation:

$$<q_{CA}^2> = R_\omega^2(0,\eta)<q_A^2>. \qquad (5.33)$$

Thus we have the result

$$R_\omega^2(0,\eta)=R_\omega^2(0,\{1-\epsilon\}\eta)R_\omega^2(0,\epsilon\eta). \qquad (5.34)$$

which has the solution

$$R_\omega(0,\eta)=e^{-\beta\eta}. \qquad (5.35)$$

Let us now look back at the assumption referred to in footnote 26. The term $<q_{CB*}^2>$ in Eq. (5.31) which has zero correlation with the signal at point B was also assumed to have zero correlation with the more remote point A. While it seems unlikely that the following situation would occur, let us suppose that some of the information contained in the turbulent eddies at point A somehow bypasses point B and

---

[26]We will come back to this point later, but for the moment let us accept it on an intuitive basis.

arrives at point C. If this situation occurs over the long-term average, then there will be a finite correlation coefficient between the signals q_{CB*} and q_A. If we represent this correlation coefficient by Δ then Eq. (5.32) takes the form,

$$<q_{CA}^2> = R_\omega^2(0,\{1-\epsilon\}\eta_1)R_\omega^2(0,\epsilon\eta_1)<q_A^2> + \Delta^2<q_{CB*}^2> \tag{5.36}$$

where we have chosen η to represent the particular distance η_1. Now if the β in Eq. (5.35) is the proper value, say β_1, to predict the correlation coefficient at the particular separation $\epsilon\eta_1$, i.e.

$$R_\omega(0,\epsilon\eta_1)=\exp(-\beta_1\epsilon\eta_1) , \tag{5.37}$$

then if Δ is greater than zero, we would have

$$R_\omega(0,\eta_1)>\exp(-\beta_1\eta_1). \tag{5.38}$$

Of course we could choose a $\beta_2<\beta_1$ such that

$$R_\omega(0,\eta_1)=\exp(-\beta_2\eta_1) \tag{5.39}$$

for the particular separation η_1. Now since $\beta_2<\beta_1$, if we replaced β_1 by β_2 in Eq. (5.37) we would obtain the relation

$$R_\omega(0,\epsilon\eta_1)<\exp(-\beta_2\epsilon\eta_1) \tag{5.40}$$

for $0<\epsilon<1$. We now have that for separations over the open interval $(0,\eta_1)$ the correlation coefficient is less than that given by the exponential of relation (5.40). If we do not wish to commit ourselves as to whether Δ in Eq. (5.36) is zero or greater than zero, we still have that the correlation coefficient in the neighborhood of zero separation is less than or equal to a particular exponential function. Therefore, since the exponential function has a finite slope at zero separation, the correlation coefficient must also have a finite slope at the origin.

The above arguments specifically apply only to the case of narrow band correlations or cross spectral densities, while the proofs of Taylor (1922) and Hinze (1959, p. 35), which say that the correlation coefficient should have a zero slope at the origin, apply to the broad-band case. It appears, however, that the broad-band correlation coefficient could be obtained by integrating the narrow-band covariance over the frequency range and then dividing by the product of the standard deviations of the individual signals. If this were done, the absolute value of the slope of the correlation coefficient versus separation, as the separation approached zero, should be at least as great as that of the frequency component that had the minimum absolute slope. This result, of course, runs directly counter to the results of Taylor and Hinze. In view of this situation, it must be realized that the arguments given above do not have the rigor usually associated with mathematical proofs. It is believed, however, that the concepts found in these arguments will be found useful, therefore it will be left to others to explore more fully the limits of application of these arguments.

D. Diagonal Correlation Coefficient

To the author's knowledge, the only correlation measurements other than those for either purely lateral or purely longitudinal separations are those by Serafini (1962) and Bull, et al. (1963). Although no theoretical justification had been given at the time, both of the above authors along with Corcos (1963) used the relation,

$$R_{opt,\omega}(\xi,\eta) = R_{opt,\omega}(\xi,0) R_{\omega}(0,\eta). \tag{5.41}$$

White (1964), on the basis of physical arguments, derives a relation

which indicates that the actual optimized correlation coefficient is very slightly larger than that predicted by Eq. (5.41).

The present data consists of four runs using a square microphone array. The runs cover a range of wind speeds from 2.4 to 6.1 meters/sec (as measured at a height of 4.27 meters). For each of the four runs, the values of correlation coefficient and optimized correlation coefficient were computed for all six combinations of pairs of microphones. Since the nominal wind direction was parallel to a side of the square array, corresponding measurements of the longitudinal correlation coefficient were obtained from each side of the array. Likewise, two values of lateral correlation coefficient were obtained from the other two sides and values of the diagonal correlation coefficient were obtained from each of the two diagonals. The small differences between corresponding values of the longitudinal and also the lateral correlation coefficients gave evidence that the turbulence was quite homogeneous over the surface of the ground. Somewhat larger differences in the correlation coefficients between the two diagonals indicated that the average wind direction was not exactly parallel to the side of the array in any of the runs. Figure 6a is a graph of correlation versus frequency for run number 08404AB,[27] showing the average diagonal correlation coefficient and the product of the average lateral and the average longitudinal correlation coefficients. The graph shows that the product approximation,

$$R_\omega(\xi,\eta) \approx R_\omega(\xi,0)R_\omega(0,\eta), \qquad (5.42)$$

is reasonably accurate.

---

[27]Graphs of the other three runs looked very much like this, although this was slightly better than average.

Since it was noted that the wind direction was not exactly parallel to one side of the array, it might be that the product approximation is even more accurate than is indicated by Fig. 6a. An estimate of the error in wind direction was obtained in the following manner. The broad band cross covariance of the two upwind microphones was plotted as a function of time delay. Now if the wind direction had been precisely at right angles to a line through these two transducers, the cross covariance should have been a maximum at zero time delay. Since the maximum occurred at a slightly different time delay, it was possible (using the average wind speed) to calculate an estimate of the error in wind direction. In the actual calculation the time delay from the two upwind transducers was averaged with the time delay obtained from the two downwind transducers.

Using the above estimated wind direction and the assumptions,

$$R_\omega(\xi,0)=e^{-\alpha\xi}\cos\frac{\omega\xi}{U_c}$$

$$R_\omega(0,\eta)=e^{-\beta\eta}$$

and
$$R_\omega(\xi,\eta)=R_\omega(\xi,0)R(0,\eta),$$

along with an assumed convection velocity of 7 meters/sec, computations were made to determine what $R_\omega(\xi,\eta)$ and $R_\omega(\xi,0)R_\omega(0,\eta)$ would have been had the wind direction been correct. This corrected plot is shown in Fig. 6b. An examination of this plot and similar plots from the other three runs reveals the following general characteristics: (1) While the product of the longitudinal and lateral correlation coefficients is a good approximation to the diagonal correlation coefficient, it is, in general, slightly lower. (2) In the region where the coherence is low (to the right of the broken line) there are relatively large random

fluctuations in the data.[28] (3) Where the data are more reliable (to the left of the broken line), the diagonal correlation coefficient and the product approximation tend to converge at the lower frequencies.

Characteristics (1) and (3) are in qualitative agreement with White's (1964) theoretical predictions. A quantitative comparison with White's theory could not be made because his results are presented (in the form of a graph) only for the case $\omega\delta/U_\infty = 10$. Also, the quantitative reliability of the present data would be somewhat marginal for such a comparison, since it depends upon taking small differences between two relatively large quantities.

Although we will not go into it here, it is interesting to note that arguments based on the principles introduced in the previous subsections can be used to show that the product approximation is either equal to or slightly less than the diagonal correlation coefficient.

E. Relationships Between Correlation Coefficient Parameters

1. Longitudinal coherence versus wave number. As seen in the previous parts of this section, the general consensus of opinion is that the longitudinal correlation coefficient can be expressed in the form

$$R_\omega(\xi,0) = A\left(\frac{\omega\xi}{U_c}\right) \cos \frac{\omega\xi}{U_c} , \qquad (5.9)$$

thus showing similarity with respect to the Strouhal number $S = \omega\xi/U_c$. A notable exception to the above is White's theory (1964) which predicts that the optimized correlation coefficient A is a function of both $\omega\xi/U_c$, and $\omega\delta/U_\infty$, where δ is the boundary layer thickness.

As seen previously, the present experiment indicates the

---

[28]Although not investigated in detail, it is believed by the author that this is inherent in the statistics of the problem.

functional form,

$$R_{\omega}(\xi,0)=e^{-\alpha\xi}\cos(k\xi). \tag{5.21}$$

We note that if the present experimental data are to agree with Eq. (5.9), α must be proportional to k. In order to explore the relation between α and k, a log-log plot (Fig. 7) was made showing the data from essentially all of the pertinent runs. Although the data represent a wide range of wind speeds and atmospheric stability conditions, the points fall into a remarkably uniform pattern.

Upon examining Fig. 7 more closely, we notice the following characteristics: The data seem to divide into two regions in the vicinity of the vertical line placed at k = .02 meters^{-1}. To the right of this line the data can be rather well represented by the line

$$\alpha = 0.41(k)^{1.28} \tag{5.43}$$

where α and k are expressed in reciprocal meters. Due to the scatter[29] of the data, one might "reasonably" represent this region with a line having a slope anywhere from 1.2 to 1.4; however, a slope of 1.0 which would be required by Eq. (5.9), is clearly a poorer approximation. In the left-hand region of the plot (k < .02), we notice that certain individual runs can be reasonably well represented by α = constant where the constant may depend upon the particular run. This last finding is in agreement with Bull.

Bull, et al. (1963) find that it is necessary to distinguish between small and large eddies; and, in particular, that for wave numbers less than k = .36/δ* (the large eddies), the coherence scale is

---

[29]The scatter in the points toward the small k (large wavelength) end of the curve is probably due to those values of α and k being computed from Coh$^{1/2}$ and R curves which cover only a small fraction of a wavelength. (See, for example, Figs. 4a - 4d.)

independent of k. If we assume that the turbulence in the present

experiment is similar to that investigated by Bull, et al., and that

the behavior of the left hand portion of Fig. 7 is the result of the

same phenomenon they observed, we can get a rough estimate of the

present boundary layer displacement thickness. Thus we have

$$k = .02 = .36/\delta^*$$

or

$$\delta^* = 18 \text{ meters.} \tag{5.44}$$

By similarly scaling the boundary layer thickness we obtain,

$$\delta \approx 200 \text{ meters.} \tag{5.45}$$

The above estimates might very well represent the average character-

istics of the present set of runs to within a factor of, perhaps, two.

Looking now at the right-hand portion of Fig. 7, we notice that

the relation $\alpha = 0.41 \, k^{1.28}$ is basically in disagreement with the

similarity relation which says that $R_\omega(\xi,0)$ is a function of $k\xi = \omega\xi/U_c$

only. In particular, we have

$$R_\omega(\xi,0) = \exp(-0.41 \, k^{1.28}\xi)\cos(k\xi) \tag{5.46}$$

which says that the coherence is a stronger function of wave number k

than of distance ξ. Turning now to Fig. 5, we see that, qualitatively

at least, this is exactly what is predicted by White's theory.

Now, from similarity considerations, one might first expect that

the longitudinal "persistence" scale $1/\alpha$ might be proportional to the

wavelength λ. However, a few simple considerations will indicate one

mechanism whereby such a similarity relation breaks down. Kraichnan

(1956a and 1956b) has shown that, for the wide-band case, the dominant

contributions to the wall pressure fluctuations come from velocity

fluctuations which are located within one or two turbulent velocity

correlation lengths of the observation point. Intuitively, there seems
to be no difficulty in extending this result to say that, for the
narrow-band case, high frequency pressure fluctuations are predominantly
due to velocity fluctuations within a distance of one or two wave
lengths corresponding to the high frequency. Likewise, low frequency
pressure fluctuations are predominantly due to velocity fluctuations
within a distance of one or two wavelengths corresponding to the low
frequency.

The deviation from similarity can be explained by considering the
interaction between large and small eddies in the turbulent flow.
Suppose the average velocity U of such a flow is in the x direction.
If a small eddy passes the point x_1 at time t=0, it will ordinarily
pass the point $x_2 = x_1 + \Delta x$ at a time $\Delta x/U$ later; if, however, there
happens to be a velocity fluctuation u_x due to a large eddy, the small
eddy will arrive at x_2 at a different time. This fluctuation in travel
time of the small eddies, due to the action of the large eddies, has
the effect of reducing the average coherence in the frequency range of
the small eddies. Now, consider a similar situation except that we
have a transverse velocity fluctuation u_y due to a large eddy instead
of the longitudinal fluctuation. In this case, a small eddy which
passes directly over the point x_1 might just graze the point x_2 or
possibly miss it entirely. Here again the effect of the large eddies
is to reduce the coherence of the small eddies between points x_1 and
x_2. Now, if we look at the effect of the small eddies upon the
coherence of the large eddy pressure fluctuations, we find that the
velocity variations due to the small eddies cannot physically displace
the large eddies and, therefore, cannot cause any phase variation in

the large eddies. The only thing the small eddies can do is to cause local high frequency pressure fluctuations which simply add to the low frequency pressure undulations due to the large eddies. Since we are measuring the narrow band correlations, the high frequency pressure fluctuations added to the low frequency variations cannot affect the coherence in a low frequency pass band.

In summary of the above, we see that longitudinal velocity fluctuations from large eddies cause phase fluctuations in the pressure signal from the small eddies, and large-eddy lateral velocity fluctuations tend to replace the small-eddy signal that would normally be present at the downstream transducer with the signal from other (uncorrelated) small eddies. The effect the small eddies have upon the large eddies is different because the small eddies cannot physically displace the large eddies. Hence, we have the result that the interaction between the eddies of various sizes causes the high frequency correlations to decay faster than would be predicted from similarity relations.

2. Longitudinal versus lateral scale. Very little systematic experimental work has been done in determining the relative longitudinal and lateral scale lengths for narrow-band correlations. Serafini (1963) found that under the conditions of his experiment (Mach number = 0.6 and average Reynolds number per foot of 3.45×10^6) the broad-band longitudinal-to-lateral scale ratio was 7.4. Bull, et al. (1963, p.24) found that for broad-band pressure fluctuations, the turbulence is very nearly isotropic for small transducer spacings. However, as the spatial separation increases, anisotropy develops; the scale in the lateral

direction exceeding that in the longitudinal direction.[30]

The present experimental data is based upon the four runs using the square array. Corresponding $Coh^{1/2}(\xi,0,\omega)$ terms from the two sides of the square parallel to the wind flow were averaged and, similarly, corresponding $Coh^{1/2}(0,\eta,\omega)$ terms from the other two sides were averaged. Since it has been previously established that the narrow-band optimized correlations may be represented by exponential curves, α's and β's were computed from the following relations:

$$Coh^{1/2}(\xi,0,\omega) = e^{-\alpha\xi} \qquad (5.47)$$

$$Coh^{1/2}(0,\eta,\omega) = e^{-\beta\eta}. \qquad (5.48)$$

If we define an integral scale of the longitudinal optimized correlation by the expression,

$$\int_{0}^{\infty} Coh^{1/2}(\xi,0,\omega)d\xi$$

we obtain

$$\int_{0}^{\infty} e^{-\alpha\xi}d\xi = \frac{1}{\alpha}.$$

Therefore, we will use $1/\alpha$ for a longitudinal scale and, similarly, $1/\beta$ for a lateral scale. (Note. Both of these scale lengths are functions of frequency.)

Figure 8 shows a plot of $1/\beta$ versus $1/\alpha$ for the four runs. The data can be represented fairly well by the line,[31]

$$\frac{1}{\beta} = 0.84 \left(\frac{1}{\alpha}\right)^{0.74} \qquad (5.49)$$

where $1/\alpha$ and $1/\beta$ are measured in meters. Thus for the longest scale

---

[30]For the longitudinal correlation coefficient, Serafini was using $R(\xi,0,\tau_{opt})$ while Bull, et al. used $R(\xi,0,0)$. This, at least to some extent, explains the wide difference in their results.

[31]Because of the scatter in the data, one might argue for an exponent anywhere from 0.65 to 0.80.

lengths measured, the longitudinal-to-lateral scale ratio is about 7; while for the shortest lengths, the ratio is about 1.6.[32]

Intuitively, it seems very likely that at still smaller scale lengths, the turbulence would become isotropic. If we extended the line $1/\beta = 0.84(1/\alpha)^{0.74}$, it would intersect the line $\beta = \alpha$ at a scale length of about 0.5 meters. It is very probable then, that for scale lengths less than 1/2 meter, the relation

$$\frac{1}{\beta} = \frac{1}{\alpha} \tag{5.50}$$

applies, while for larger scale lengths Eq. (5.49) is a good approximation. The above relations might be made applicable to the general boundary layer problem by scaling the dimensions to the previously estimated values of δ or δ^*.

If we eliminate α between Eq. (5.43) and Eq. (5.49), we obtain the relation

$$\beta = 0.62(k)^{0.95} \tag{5.51}$$

for β and k in reciprocal meters. By invoking the tolerance limits on the exponents of the two initial equations, we see that the relation

$$\beta \approx k \tag{5.52}$$

is well within experimental error. Thus, within the limits of the present data, we have similarity between the lateral correlation scale and the longitudinal wavelength (but not between the longitudinal scale and the longitudinal wavelength).

Now, since virtually all of the other experimenters are in agreement with this result concerning the lateral similarity, it is of great

---

[32]The range of scale lengths reported is limited purely by the sizes of the square arrays used. Both larger and smaller arrays would have been used had time permitted.

interest to see what White's theory predicts since he alone is in agreement with the present longitudinal "nonsimilarity". White (1964, Fig. 5) shows a family of curves for

$$R_\omega(0,\eta) = B\left(\frac{\omega\eta}{U_\infty} , \frac{\omega\delta}{U_\infty}\right)$$

versus $\omega\eta/U_\infty$; giving one curve for each different value of the parameter $\omega\delta/U_\infty$. The curves are crowded very close together, showing only a small variation with the parameter $\omega\delta/U_\infty$. Although White uses free stream velocity rather than convection velocity, it seems apparent that his theory does predict a "near similarity" for the lateral correlations. This is in agreement with the present findings.

3. **Convection velocity versus wavelength.** Corcos (1964) has pointed out, using the data of Willmarth and Wooldridge, that the narrow-band convection velocity is a weak function of transducer spacing and a strong function of frequency. The fact that the convection velocity was a function of transducer spacing at all, was probably an artifact of the finite frequency bandwidth of the data, which was approximately one octave. Under this assumption, then, the convection velocity is a unique function of the turbulence and not a function of the method of measurement; i.e., transducer spacing.

Although the convection velocity is typically plotted as a function of normalized frequency, we choose a somewhat different approach. As was pointed out previously in the discussion on longitudinal coherence versus wave number; it is probably safe to assume that the dominant influence of an eddy extends a distance approximately proportional to the "size" of that particular eddy. Thus we would expect the high frequency portion of the fluctuating pressure, the part arising from

small eddies, to be caused predominantly by turbulence near the ground.

Likewise, the effective source height of the low frequencies should be

expected to be higher since the larger eddies extend to a greater height.

It this is true, the "size" of the eddy versus the convection velocity

should be monotonically related to the height versus wind speed. That

is to say, if we let convection velocity correspond to wind speed, than

the wavelength should be monotonically related to source height.

The convection velocities in this experiment were obtained from the

runs using the linear array parallel to wind direction. They were com-

puted from the relation $k = \omega/U_c$. Figure 9 is a plot relating convection

velocity to wavelength where the velocities are plotted on the horizontal

axis and the wavelengths are shown along the left-hand vertical axis. A

free-band curve has been drawn to indicate the general trend of the data.

In order to arrive at a possible indication of wind profile, we

introduce the anemometer data. The anemometer at the 4.27 meter height

indicated a wind speed 2.1 m/sec. If we plot this wind speed, we notice

that it intersects the curve at a wavelength of 22 meters. Therefore, on

the basis of our modified Taylor's hypothesis, we see that the effective

source height of the 22 meter wavelength disturbance is 4.27 meters and

its velocity is 2.1 m/sec. On this basis we conclude that the wavelength

is 5.1 times the effective source height, for the disturbance of this

wavelength. Fortunately, corresponding data from a 10 meter high Weather

Bureau anemometer was also available at the time of this run.[33] The

Weather Bureau anemometer was located on a mast 90 meters from the site

of the experiment. Similar treatment of the data from the 10 meter high

---

[33]Run number 95203A was the only pertenant run for which the 10
meter anemometer data was available.

anemometer, indicates that 55 meter wavelength disturbances are being

convected at a velocity of 3 m/sec. Therefore, these disturbances have

a wavelength 5.5 times the effective source height. Using a ratio of

5.3, we can draw a scale along the right-hand side of the graph and

name it a "height" scale. On the basis of this sketchy evidence, one

might even be tempted to call the curve a wind profile.

In reality, the evidence given above is far too meager to draw the

conclusion that the effective source height is linearly related to the

wavelength of the disturbance. Intuitively, however, it seems quite

reasonable that the two should be monitonically related; in fact, it is

not inconceivable that this functional relationship might be unique.

If, indeed, this is the case, such a relationship should prove to be

extremely useful.

Figure 9 is fairly typical of the data for which the solar radia-

tion was very low. Figure 10 shows a convection velocity plot which is

typical of the data made during conditions of high solar radiation.[34]

Under conditions of high solar radiation, the atmosphere is usually very

unstable in which case there is a great deal of vertical motion of the

air masses. Since, under these conditions, there is much mixing of

momenta between the air at different heights, we would expect the wind

profile to be quite constant except very near the ground. This is

qualitatively in agreement with the shape of the plot in Fig. 10.

---

[34]In Fig. 10 the wind speed reading from the 4.27 meter high
anemometer is plotted at a wavelength corresponding to 5.3 times its
height.

SECTION VI

POWER SPECTRA

The most relevant theoretical works which predict the shape of the wall-pressure power spectrum are the recent papers of Gardner (1963) and White (1964). Gardner assumes an inertial subrange and a one-seventh power law wind profile. After making several other approximations to facilitate integration, he concludes that the spectrum is proportional to the -3 power of the frequency. White, whose work is based upon that of Gardner, makes the same inertial subrange and wind profile assumptions; but, in place of some of the approximations of Gardner, he performs numerical integrations with the aid of a computer. White's results are reproduced in Fig. 11. This curve, which shows a gradual curvature, changes slope from about -0.2 to -3 over the range shown.

The power spectra in the present experiment were, for each run, derived from averaging the data from each of the four microphones. The spectra plots were normalized by adjusting the curves vertically for the best relative fit within the frequency range where the high frequency and the low frequency band pass data overlap, .0271 to .352 Hz. Figure 12 shows the normalized power spectra of the more representative data. The absolute power spectral density for any run may be obtained by multiplying the relative power density by the absolute power density scaling factor shown on the graph. The absolute power density scaling factor is, thus, a measure of relative power of an individual run.

The slopes of the various spectral plots, as shown on a log-log plot, were computed on the basis of a best least squares fit. Only those points for frequencies above .0271 Hz were used because some of the spectral plots tended to bend over below this frequency. The runs for which this computation [35] was made are shown in Table 4, arranged in order of spectral slopes. The slopes range from -1.64 to -2.40 with a slope of about -1.8 being representative. It is difficult to make a direct comparison between White's theory and the data because δ and U_∞ are not well known for the data. We can, of course, by taking some liberty, compare only the shape of White's curve with the data. Upon doing this we find that the fit is only fairly good; the curvature of White's curve is too great to match the one and a half decade linear portion of the present data. A more realistic approach might be to go ahead and use the best estimates of δ and U_∞ to line up the abscissa and then fit the ordinate. Since the wind speeds (measured at a height of 4.27 meters) of the various runs are weighted heavily in the region of 5 to 6 meters per second, we will guess that the "typical" free stream velocity might be in the order of 10 meters per second. For the boundary layer thickness we will use the value estimated in the last section; i.e., δ=200 meters. If we take the center of the band of the present data, say 0.1 Hz, as a point of reference, we obtain a nondimensional frequency of $\omega\delta/U_\infty$=12.6. If we now look at White's curve (Fig. 11), we find that this places the center of our measured

---

[35]The data taken with the square arrays had to be omitted from consideration in this section. The temperature during these runs was so low the calibration could not be trusted.

spectra at the right-hand end of the curve. Indeed, (by extrapolation) this is an almost linear portion of White's curve. However, the slope of White's curve is -3 in this region, while the slope of the present spectra is about -1.8.

We might now turn our attention toward the experimental results of others. In the atmosphere Gossard (1960) found that in the range 0.1 to 5 Hz the spectral slope was about -2. In the frequency range of 0.033 to 1 Hz Richie (1965) found a spectral slope of about -2 in both low winds and high winds (0 to 4 knots and 20 to 30 knots). Both of these works are considered to be in quite good agreement with the present data.

The wind tunnel data is, unfortunately, not very consistent. If we use the previously mentioned parameters to convert the frequency scale of the present data into dimensionless form, we may compare it with that of several other experimenters by matching the dimensionless frequency scales and moving the data vertically to obtain the best fit. If we do this, the data of Bull, et al. (1963) match very well, the data of Willmarth and Wooldridge (1962) match fairly well if we apply Corcos's (1963) resolution correction, and the data of Serafini (1962) match fairly well if we consider only the data taken with his smallest transducer. The wind tunnel data of Harrison (1958) and the water tunnel data of Skudrzyk and Haddle (1960) show a slope of -3 in agreement with the theory of Gardner (1963), but at complete variance with the present data. The data of Bakewell, et al. (1962) agrees fairly well with the theory of White, but, alas, not with the present data.

In an attempt to explain the present data, let us note the following characteristics:

1. Each individual spectrum (on a log-log plot) is remarkably linear for a decade or more and has an absolute slope substantially less than the theoretically predicted slope for the linear portion of the curve.

2. The low frequency end of the spectra tends to bend down slightly from the slope exhibited by the linear portion of the curve.

3. Though the linear portion of each curve exhibits a unique slope (power law), the slopes of the individual power spectra range from -1.64 to -2.40.

In looking at the first characteristic, let us assume that the theories of Gardner (1963) and White (1964) are correct if the regime under consideration is far into the inertial subrange. A possible explanation is the following. MacCready (1962) found that for velocity fluctuations in a boundary layer the smallest height at which observations could be considered in the inertial subrange was about 0.6 wavelengths of the disturbance under consideration. We saw in the last section that it was reasonable to assume that the dominant contributions to the narrow-band wall-pressure fluctuations came from within distances of one or two wavelengths of the particular disturbance involved.

The above two considerations imply that a significant portion of the pressure seen at a point on the wall is due to velocity fluctuations which are not within the inertial subrange. Furthermore, since the region close to the wall (ground in the present case) is a region of high shear, it might be expected that eddies of various sizes would

be generated here. If it is true that eddies throughout the size range
being considered are being generated in the layer of high shear, then
the wall-pressure spectrum would be expected to have an absolute slope
less than that predicted for the inertial subrange. The subsection on
longitudinal versus lateral scale lengths indicates that, indeed, the
pressure fluctuations are not originating in an isotropic region.

It is difficult to determine exactly what is causing the third
characteristic, the variation in slope between runs. Table 4 lists
the runs in order of the power spectral slopes. There seems to be
substantial correlation between the spectral slope and solar radiation
and, somewhat, less correlation between spectral slope and wind speed.
An increase in wind speed would increase the Reynolds number, but it
is not clear what effect this would have upon the slope of the power
spectrum plot. An increase in solar radiation would ordinarily have
the effect of decreasing the stability of the atmosphere. Lumley and
Panofsky (1964) state that energy is fed into or out of the turbulence
depending upon whether conditions are stable or unstable, respectively.
If some of the energy being fed into the turbulence is broad band,
then this would be expected to lessen the steepness of the spectral
slope. This is in agreement with the trend as shown in Table 4.

SECTION VII

CONCLUSIONS

In the conclusions that follow, the specific results of this investigation will be pointed out with brief comments where appropriate.

1. The narrow-band longitudinal correlation coefficient can be expressed as the product of an optimized correlation coefficient and a cosine variation. Thus we have

$$R_\omega(\xi,0) = R_{\omega,opt}(\xi,0) \cos k\xi.$$

This relation has long been recognized.

2. The optimized longitudinal correlation coefficient may be represented, well within experimental error, by an exponential function; i.e.,

$$R_{\omega,opt}(\xi,0) = e^{-\alpha\xi}.$$

While the data of many workers tend to indicate an exponential curve, few of the experimenters have expressed their results in exponential form. This might well be due to the generally held concept that the slope of the correlation coefficient should tend to zero as the separation becomes small.

3. The data also indicate that the lateral correlation coefficient may be expressed as an exponential function; i.e,

$$R_\omega(0,\eta) = e^{-\beta\eta}.$$

The general situation on this point is similar to that of the optimized longitudinal correlation coefficient.

51

4. Plausibility arguments are given which indicate that both the lateral correlation coefficient and the optimized longitudinal correlation coefficient should fall off exponentially or at least almost exponentially. In any case the arguments predicted that the slope should approach a finite limit as the separation becomes small. Although the arguments are not rigorous in the mathematical sense, it is hoped that they will yield some insight into the disagreement between theory and experiment.

5. The diagonal correlation coefficient is very slightly larger than the product of the longitudinal and the lateral correlation coefficients; the difference increases with normalized frequency. This represents the first experimental verification, although only qualitative, of White's theory on this point.

6. For the longitudinal correlation coefficient $R_\omega(\xi, 0) = e^{-\alpha \xi} \cos k\xi$, the relation

$$\alpha = 0.41 \; k^{1.28},$$

where α and k are measured in reciprocal meters, is a good approximation over most of the frequency range. At the very low end of the frequency range, α tends to become constant. By scaling the above "frequency of demarcation" to the frequency at which Bull, et al., observed a similar phenomenon, we conclude that the boundary layer thickness δ in the present experiment was in the order of 200 meters.

The first part of this conclusion, α not proportional to k, represents the first time that this longitudinal "nonsimilarity" has been found experimentally. The deviation from similarity is in the direction predicted by White.

7. Over a range of longitudinal scale $1/\alpha$ from 3 to 500 meters, the longitudinal and lateral scales can be reasonably well related by the expression

$$\frac{1}{\beta} = 0.84 \left(\frac{1}{\alpha}\right)^{0.74},$$

where both scales are measured in meters. It is highly probable that at a scale length less than about 0.5 meters, the turbulence becomes isotropic and, thereafter, the expression $\alpha = \beta$ holds, although this was not measured.

Although the results shown in conclusions 6 and 7 apply particularly to the atmospheric case, the results can be made more generally applicable by scaling them on the basis of a boundary layer thickness of roughly 200 meters.

8. A method is given which, upon refinement, might provide a means of determining the wind profile from correlation measurements on the ground.

9. The power density spectra plotted on a log-log scale are remarkably linear over a frequency range of one and a half decades. The slopes range from 1.6 to 2.4 for the various runs. At the low frequency end of the spectrum the curves tend to flatten. If the frequency at which this occurs is scaled to the frequency at which a similar flattening appears in the data of Bull, et al., we again arrive at a boundary layer thickness in the order of 200 meters for the present experiment.

The slopes of the power spectra measured here are in good agreement with other experimenters' atmospheric results and some of the results of wind tunnel experiments. The agreement with the spectrum predicted by Gardner is poor while the agreement with that predicted by White's theory is a little better.

10. The variation in slope of the power spectra for the individual runs tends to correlate with the hemispheric solar radiation: the steeper slope being associated with the smaller radiation. This behavior is in the direction one would expect on the basis of atmospheric stability.

<div align="center">Table 1. List of Runs</div>

Run number	Date	Starting time of run (LST)	Run time (min)	Pass band	Microphone array	Nominal wind direction relative to array	Standard deviation of wind direction	Wind speed at 4.27 m height (m/sec)	Standard deviation of wind speed (m/sec)	Hemispheric solar radiation cal/cm² hr	Temp. °F	Dew point °F	Total sky cover (tenths)	Visibility at surface (statute miles)	Remarks
					Linear										
65202AB	11-5-64	12:10 PM	20	Hi	Small	‖	8°	5.4	.76	44	72	46	3	8	Scattered clouds at 5,000 ft.
68202AB	11-5-64	3:10 PM	20	Hi	Large	‖	10°	5.6	.98	16	71	43	3	8	Scattered clouds at 5,000 ft.
70502AB	11-5-64	5:40 PM	20	Hi	Large	⊥	8°	3.6	.63	~ 2	65	38	0	10	
71202AB	11-5-64	6:10 PM	20	Hi	Large	⊥	8°	5.6	1.03	· 0.2	64	36	0	10	
73202A	11-5-64	7:40 PM	40	Lo	Large	⊥	11°	4.9	.98	.0	64	34	0	10	
74402B	11-5-64	9:40 PM	40	Lo	Large	45°	8°	5.1	.89	0	54	35	0	10	
78002B	11-6-64	1:00 AM	40	Lo	Large	45°	11°	3.1	.67	.0	51	33	0	10	
91203A	11-6-64	1:40 PM	40	Lo	Large	‖	12°	7.2	1.52	~ 24	56	37	9	15 +	Scattered clouds at 4,000 ft.
92403A	11-6-64	3:00 PM	40	Lo	Large	‖	10°	6.0	1.25	~ 25	56	37	5	15 +	Scattered clouds at 4,000 ft
92403B	11-6-64	3:40 PM	40	Lo	Large	‖	10°	4.9	.98	~ 22	56	35	0	15 +	
94003A	11-6-64	4:20 PM	40	Lo	Large	‖	9°	3.8	.72	~ 5	52	37	0	15 +	
95203A	11-6-64	5:40 PM	40	Lo	Large		10°	2.1	.31	0.1	51	35	0	15 +	
					Square										
69201AB	2-9-65	4:10 PM	20	Hi	6.10 m	‖ to side	5	2.4	.30	2	45	36	10	8	Light rain. clouds at 2,000 ft.
06103AB	2-27-65	1:00 AM	20	Hi	9.15 m	‖ to side	8°	4.9	.83	0	22	7	0	15 +	
07503AB	2-27-65	2:40 AM	20	Hi	9.15 m	‖ to side	7°	4.5	.56	.0	21	6	0	15 +	
09403B	2-27-65	3:30 AM	20	Hi	9.15 m	‖ to side	8°	6.1	.88	.0	21	3	0	15 +	

Table 2. Low Frequency Pass-Band Grouping of Frequency Components for Converting from a Linear to a Logarithmic Frequency Scale
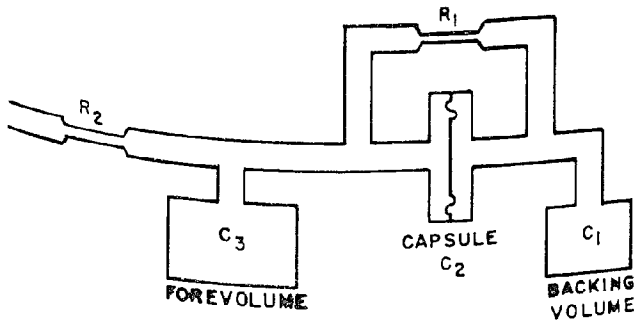
Number of frequency components within each group	Frequency components of original linear scale (Hz)	Center frequencies of nominal 1/3-octave bands (Hz)
1	.00417	not used
1	.00833	.00833
1	.0125	.0125
1	.0167	.0167
1	.0208	.0208
1	.0250	.0250
2	.0292 .0333	.0312
2	.0375 .0417	.0395
3	.0458 .0500 .0542	.0498
4	.0583 : .0708	.0642
4	.0750 : .0875	.0810
5	.0916 : .108	.100
7	.113 : .137	.125
9	.142 : .175	.157
11	.179 : .221	.199
14	.225 : .279	.250
17	.283 : .350	.315
36	.354 : .500	not used

Table 3. High Frequency Pass-Band Grouping of Frequency Components for Converting from a Linear to a Logarithmic Frequency Scale

Number of frequency components within each group	Frequency components of original linear scale (Hz)	Center frequencies of nominal 1/3-octave bands (Hz)
1	.0167	not used
1	.0333	.0333
1	.0500	.0500
1	.0667	.0667
1	.0833	.0833
1	.100	.100
2	.117 .113	.125
2	.150 .167	.158
3	.183 .200 .217	.199
4	.233 ⋮ .283	.257
4	.300 ⋮ .350	.324
5	.367 ⋮ .433	.399
7	.450 ⋮ .550	.497
9	.567 ⋮ .700	.630
11	.717 ⋮ .883	.796
14	.900 ⋮ 1.117	1.00
17	1.133 ⋮ 1.400	1.260
36	1.417 ⋮ 2.000	not used

Table 4. Power Spectral Parameters and Related Variables

Run number	Slope of spectrum on log-log plot	Absolute power density scaling factor $\left(\dfrac{\mu bar^2}{rad/sec}\right)$	Wind speed (meters/sec)	Hemispheric solar radiation (Langleys/hr)
65202AB	-1.64	21.8	5.4	44
92403A	-1.67	21.3	6.0	25
92403B	-1.70	7.23	4.9	22
91203A	-1.71	43.4	7.2	24
68203AB	-1.85	25.3	5.6	15
74402B	-1.87	9.65	5.1	0
94002B	-1.89	3.25	3.8	5.3
78002B	-2.11	2.65	3.1	0
95203A	-2.40	0.75	2.1	0.1

59

Fig. 1a. Schematic diagram of microphone assembly.

$C_1 = .00374 \ \dfrac{cm^5}{dynes}$

$C_2 = .0055 \ \dfrac{cm^5}{dynes}$

$C_3 = .018 \ \dfrac{cm^5}{dynes}$

$R_1 = 70.7 \ \dfrac{cm^5}{dynes\text{-}sec}$

$R_2 = 16.7 \ \dfrac{cm^5}{dynes\text{-}sec}$

Fig. 1b. Electrical equivalent circuit of microphone assembly.
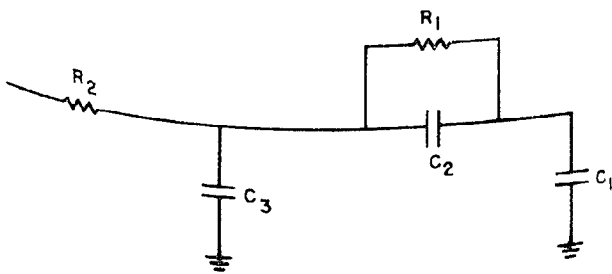
$C_1 = 3.74$ millifarads

$C_2 = 5.5$ millifarads

$C_3 = 18.7$ millifarads

$R_1 = 70.7$ ohms

$R_2 = 16.7$ ohms
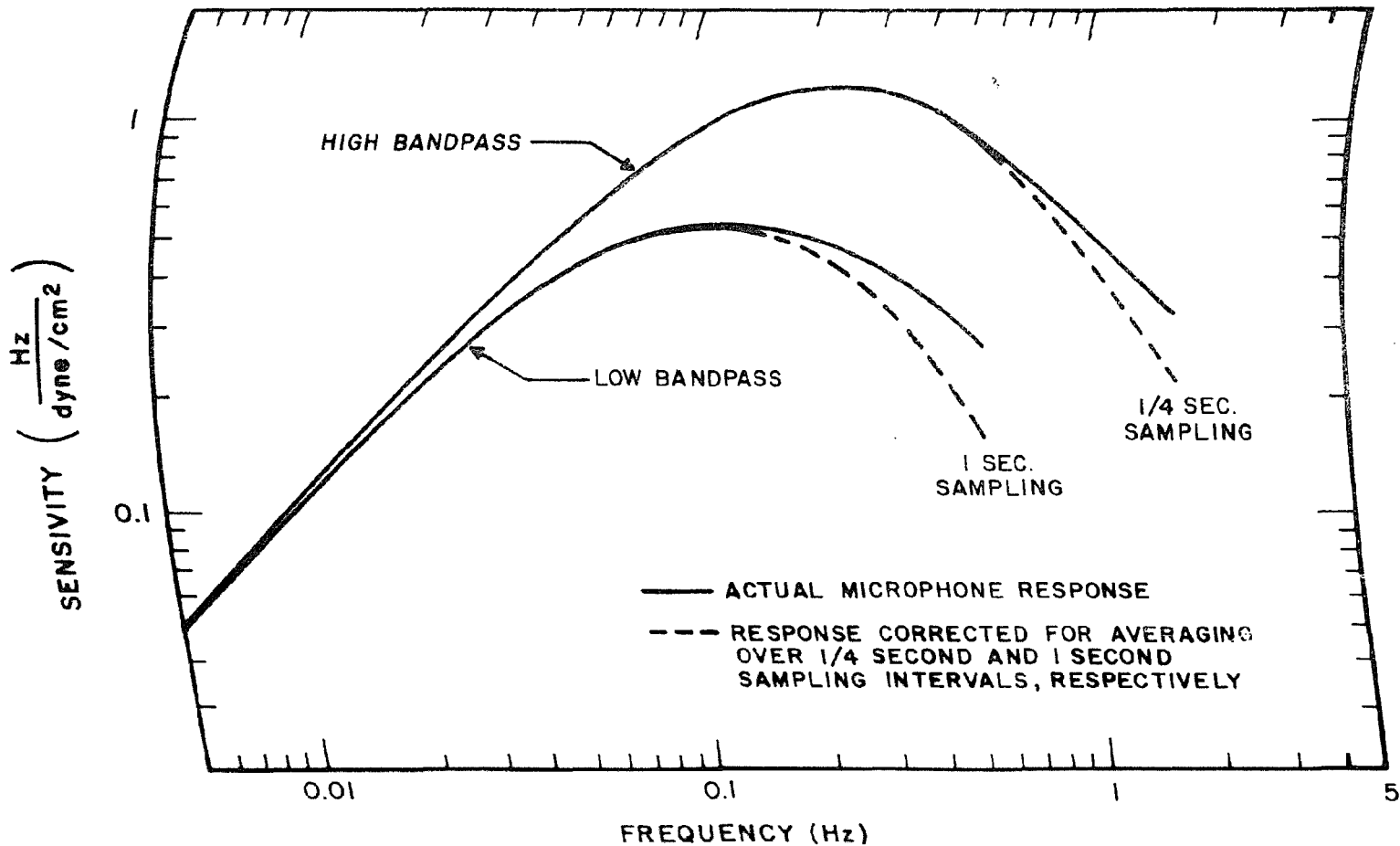
Fig. 2. Average frequency response of the four microphones
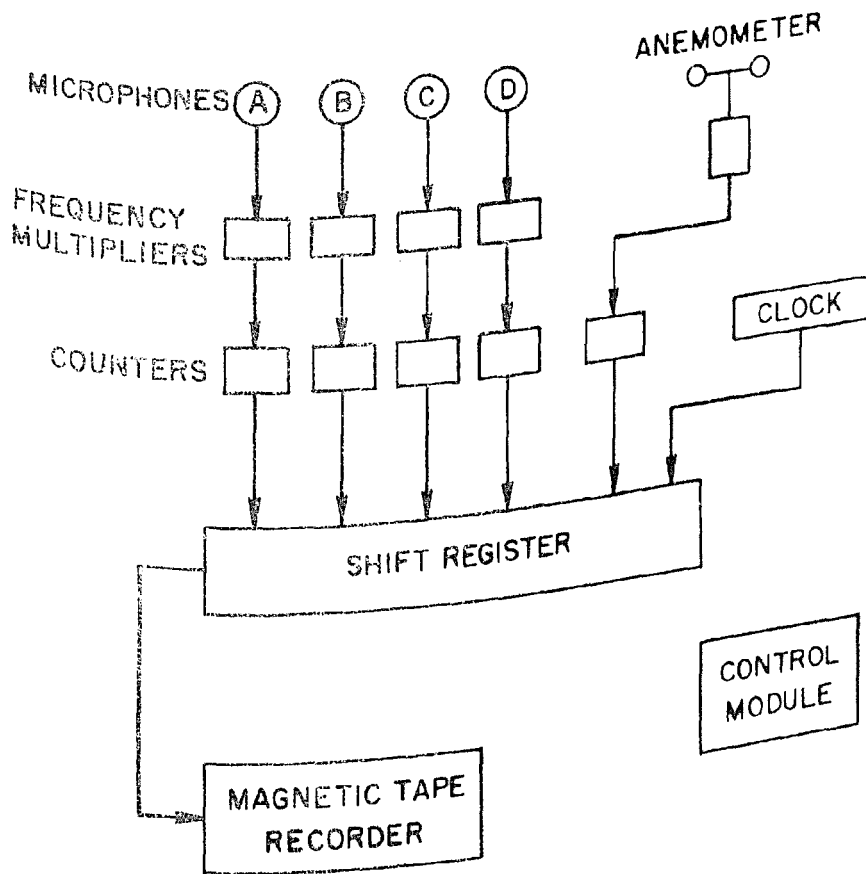
Fig. 3. Block diagram of digital recording system.

(4a)

$f_o = .00833$ Hz
$\alpha = .00186$ Meters^{-1}
$k = .00933$ Meters^{-1}

$\triangle$ Coh$^{\frac{1}{2}}(\xi)$
$\bigcirc$ R (ξ)

ξ (Meters)

(4b)

$f_o = .0125$ Hz
$\alpha = .00178$ Meters^{-1}
$k = .0106$ Meters^{-1}

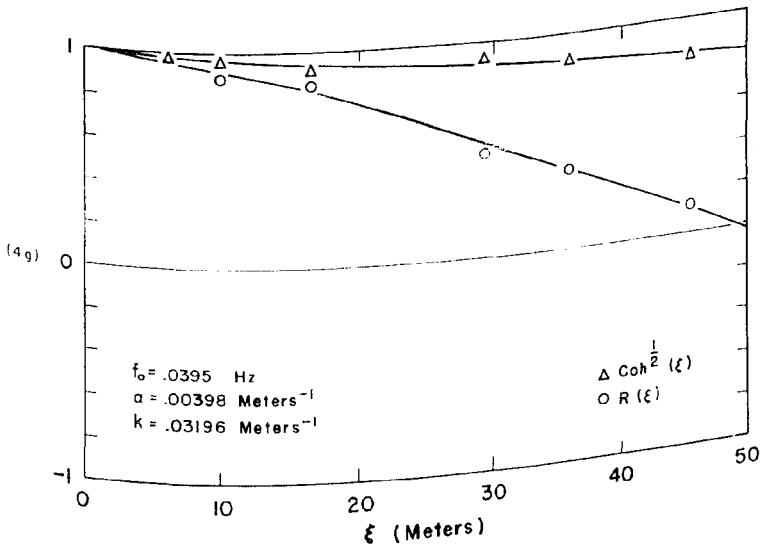$\triangle$ Coh$^{\frac{1}{2}}(\xi)$
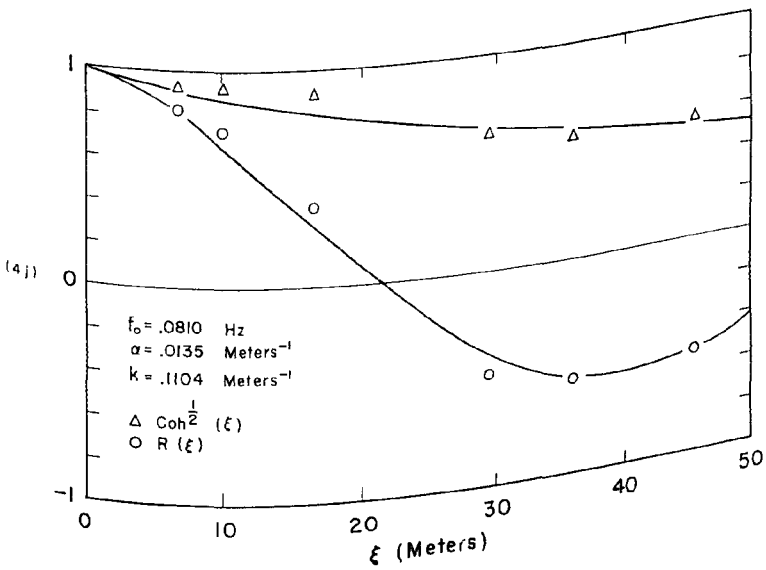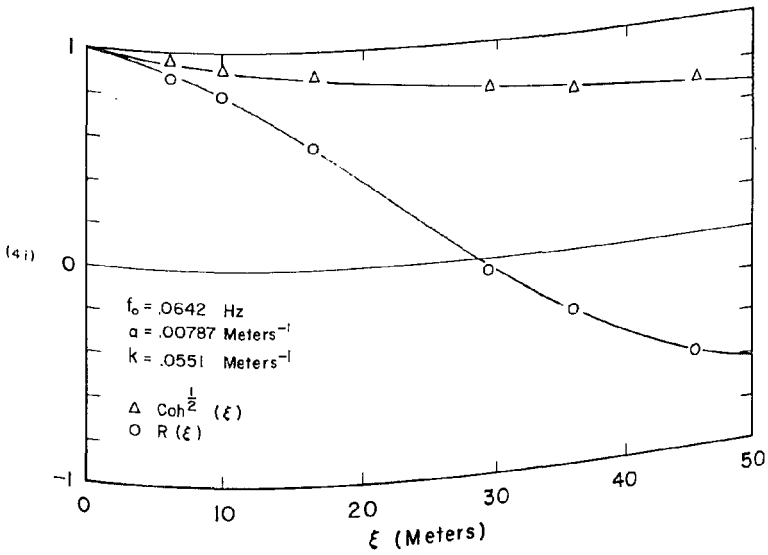$\bigcirc$ R (ξ)

ξ (Meters)
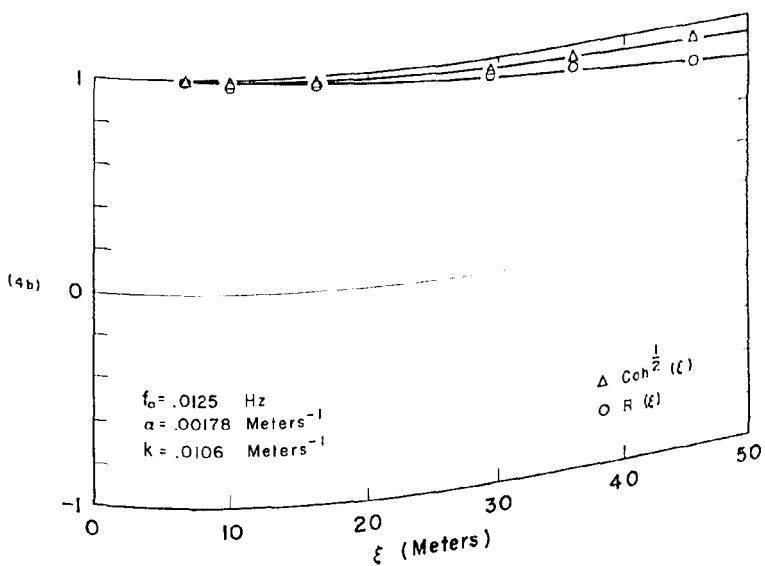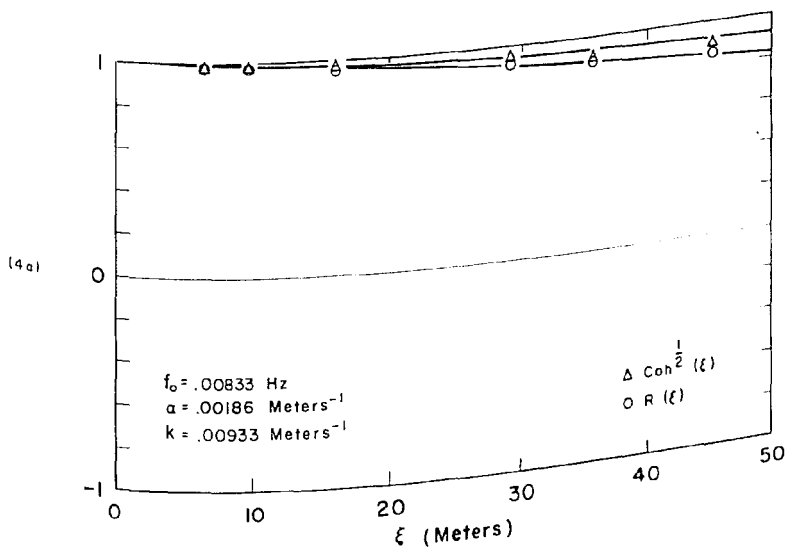
Figs. 4a and 4b. Longitudinal correlation coefficient and optimized longitudinal correlation coefficient versus separation for the $\frac{1}{3}$ –octave band centered at f_o. The upper and lower curves in each graph are respectively $e^{-\alpha\xi}$ and $e^{-\alpha\xi}\cos k\xi$ where α and k were derived from the best least squares fit to the data. Run number 92403 A.
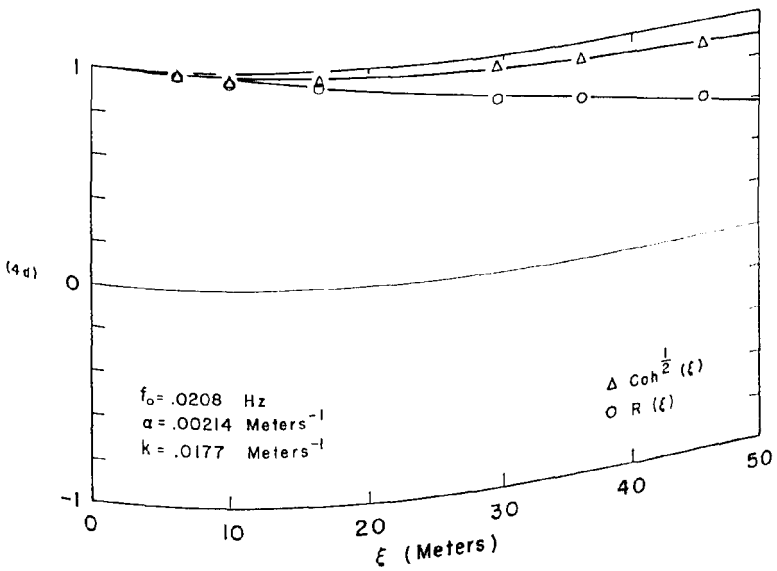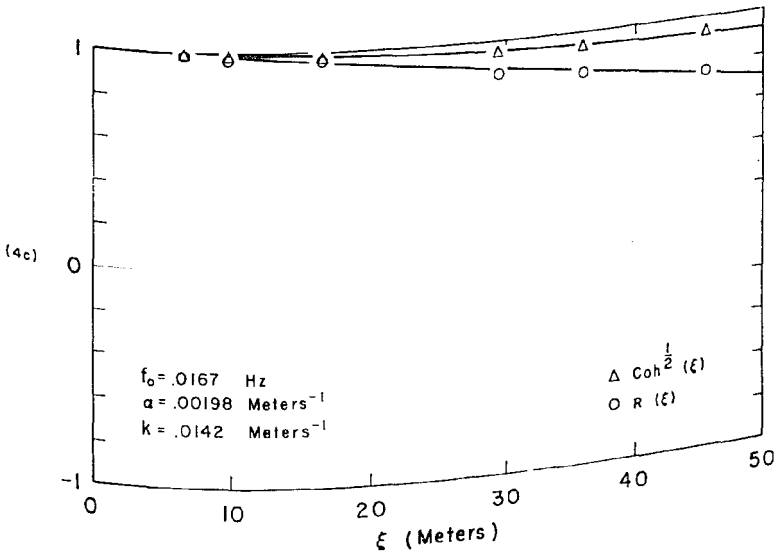
Figs. 4c and 4d. Longitudinal correlation coefficient and optimized longitudinal correlation coefficient versus separation for the ⅓ −octave band centered at f_o. The upper and lower curves in each graph are respectively $e^{-a\xi}$ and $e^{-a\xi}\cos k\xi$ where a and k were derived from the best least squares fit to the data. Run number 92403 A.

(4e)

$f_o = .0250$ Hz
$a = .00219$ Meters^{-1}
$k = .0234$ Meters^{-1}

$\triangle$ Coh$^{\frac{1}{2}}$ (ξ)
O R (ξ)

ξ (Meters)

(4f)

$f_o = .0312$ Hz
$a = .00221$ Meters^{-1}
$k = .0273$ Meters^{-1}

$\triangle$ Coh$^{\frac{1}{2}}$ (ξ)
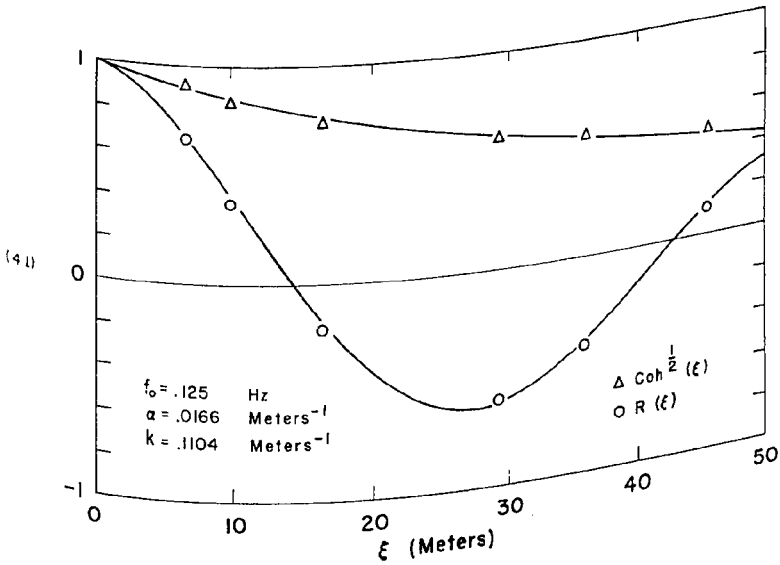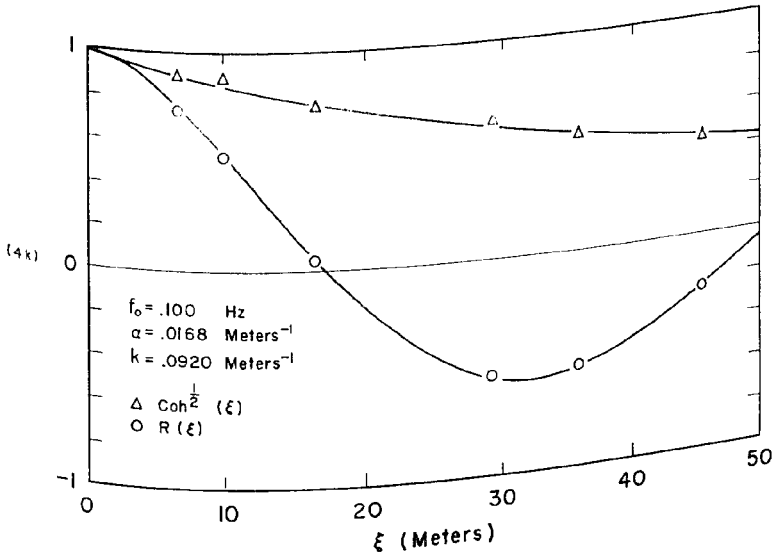O R (ξ)

ξ (Meters)
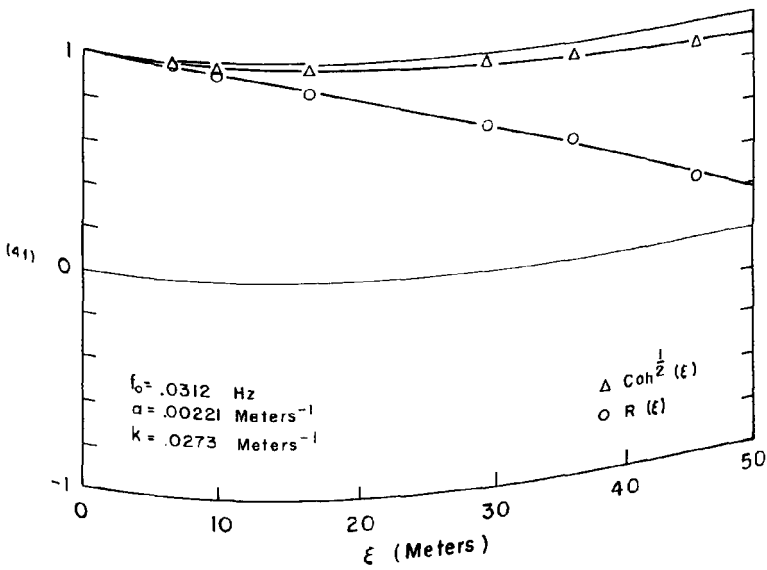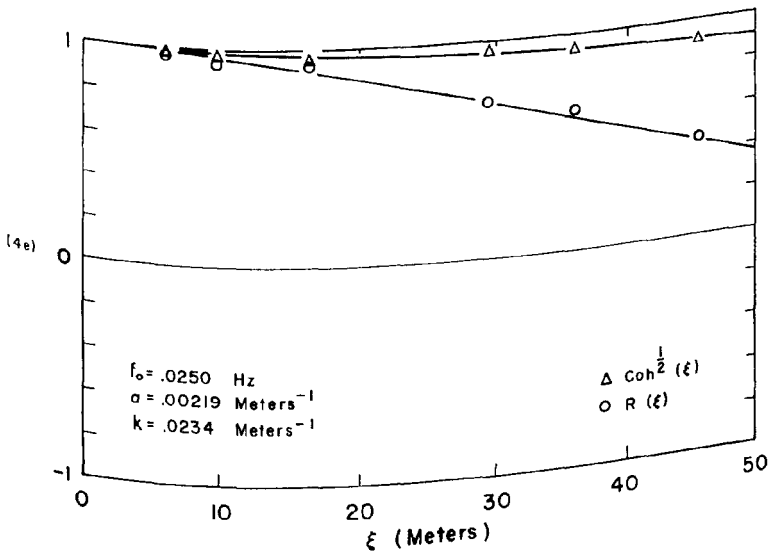
Figs. 4e and 4f. Longitudinal correlation coefficient and optimized longitudinal correlation coefficient versus separation for the $\frac{1}{3}$ -octave band centered at f_o. The upper and lower curves in each graph are respectively $e^{-a\xi}$ and $e^{-a\xi}\cos k\xi$ where a and k were derived from the best least squares fit to the data. Run number 92403 A.
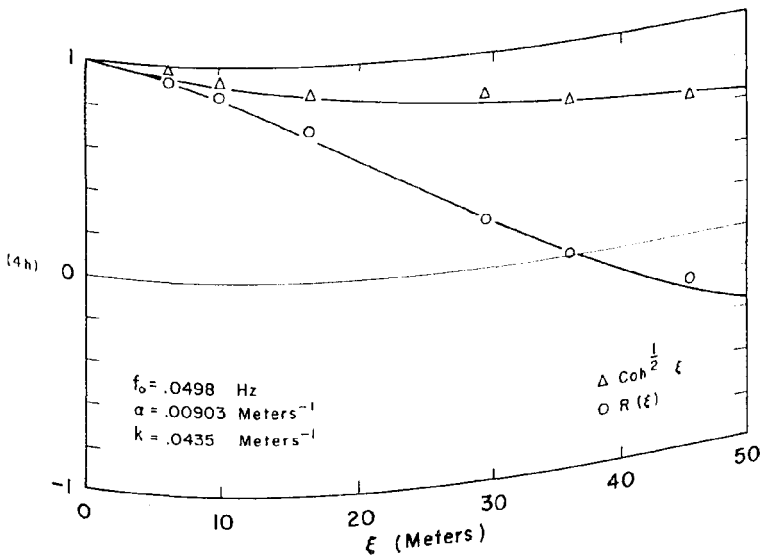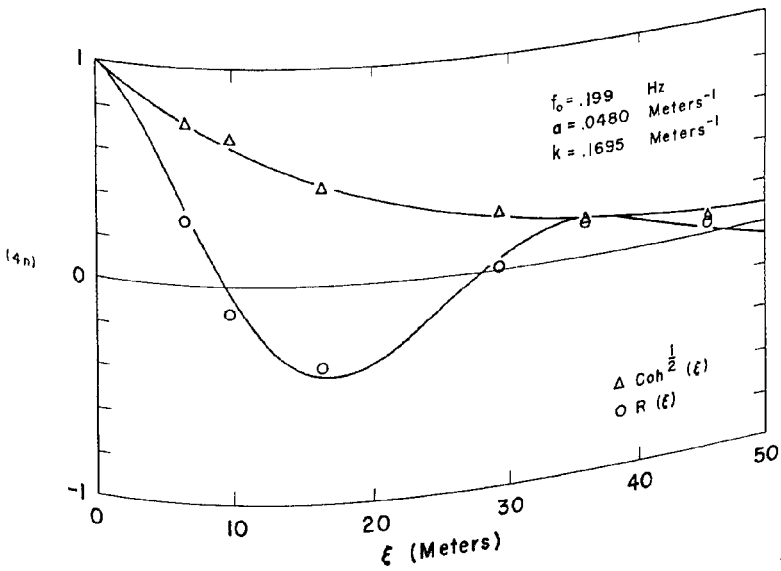
Figs. 4g and 4h. Longitudinal correlation coefficient and optimized longitudinal correlation coefficient versus separation for the $\frac{1}{3}$ -octave band centered at f_o. The upper and lower curves in each graph are respectively $e^{-\alpha\xi}$ and $e^{-\alpha\xi}\cos k\xi$ where α and k were derived from the best least squares fit to the data. Run number 92403 A.

(4 i)

$f_o = .0642$ Hz
$a = .00787$ Meters^{-1}
$k = .0551$ Meters^{-1}

△ Coh$^{\frac{1}{2}}$ (ξ)
O R (ξ)

ξ (Meters)

(4 j)

$f_o = .0810$ Hz
$\alpha = .0135$ Meters^{-1}
$k = .1104$ Meters^{-1}

△ Coh$^{\frac{1}{2}}$ (ξ)
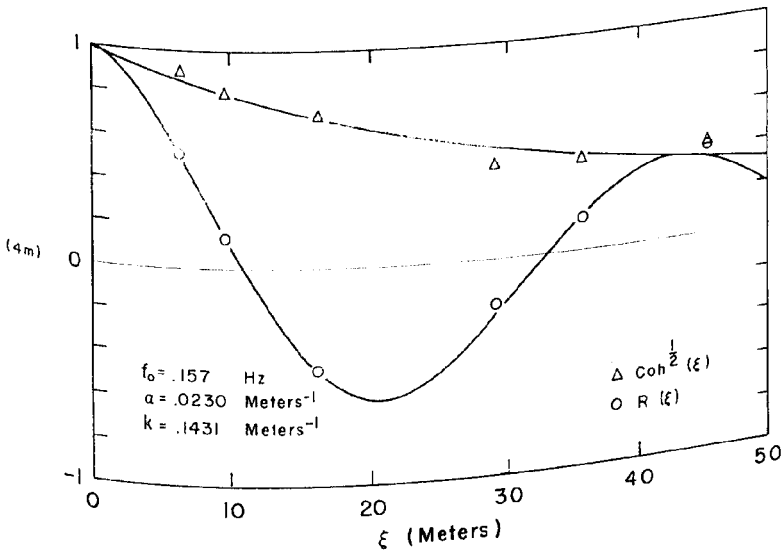O R (ξ)

ξ (Meters)

Figs. 4 i and 4 j. Longitudinal correlation coefficient and optimized longitudinal correlation coefficient versus separation for the $\frac{1}{3}$ -octave band centered at f_o. The upper and lower curves in each graph are respectively $e^{-\alpha\xi}$ and $e^{-\alpha\xi}\cos k\xi$ where α and k were derived from the best least squares fit to the data. Run number 92403 A.
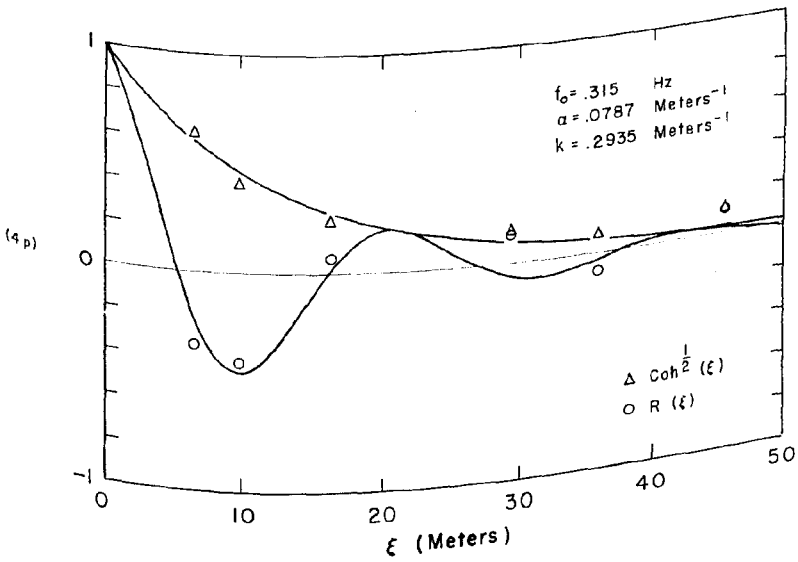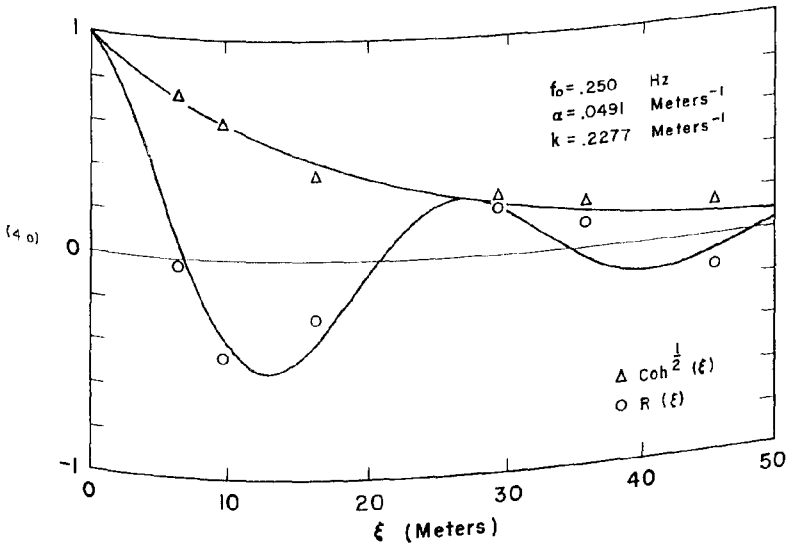
Figs. 4k and 4l. Longitudinal correlation coefficient and optimized longitudinal correlation coefficient versus separation for the $\frac{1}{3}$ -octave band centered at f_o. The upper and lower curves in each graph are respectively $e^{-\alpha\xi}$ and $e^{-\alpha\xi}\cos k\xi$ where α and k were derived from the best least squares fit to the data. Run number 92403 A.

(4m)

$f_o = .157$ Hz
$a = .0230$ Meters^{-1}
$k = .1431$ Meters^{-1}

$\triangle$ Coh$^{\frac{1}{2}}(\xi)$
O R (ξ)

ξ (Meters)

(4n)

$f_o = .199$ Hz
$a = .0480$ Meters^{-1}
$k = .1695$ Meters^{-1}

$\triangle$ Coh$^{\frac{1}{2}}(\xi)$
O R (ξ)

ξ (Meters)

Figs. 4m and 4n.   Longitudinal correlation coefficient and optimized longitudinal correlation coefficient versus separation for the $\frac{1}{3}$ -octave band centered at f_o. The upper and lower curves in each graph are respectively $e^{-a\xi}$ and $e^{-a\xi}\cos k\xi$ where a and k were derived from the best least squares fit to the data Run number 92403 A.

(4 o)

$f_o = .250$ Hz
$\alpha = .0491$ Meters^{-1}
$k = .2277$ Meters^{-1}

$\triangle$ Coh$^{\frac{1}{2}}$ (ξ)
O R (ξ)

ξ (Meters)

(4 p)

$f_o = .315$ Hz
$\alpha = .0787$ Meters^{-1}
$k = .2935$ Meters^{-1}

$\triangle$ Coh$^{\frac{1}{2}}$ (ξ)
O R (ξ)

ξ (Meters)

Figs. 4o and 4p. Longitudinal correlation coefficient and optimized longitudinal correlation coefficient versus separation for the $\frac{1}{3}$-octave band centered at f_o. The upper and lower curves in each graph are respectively $e^{-\alpha\xi}$ and $e^{-\alpha\xi}\cos k\xi$ where α and k were derived from the best least squares fit to the data. Run number 92403 A.
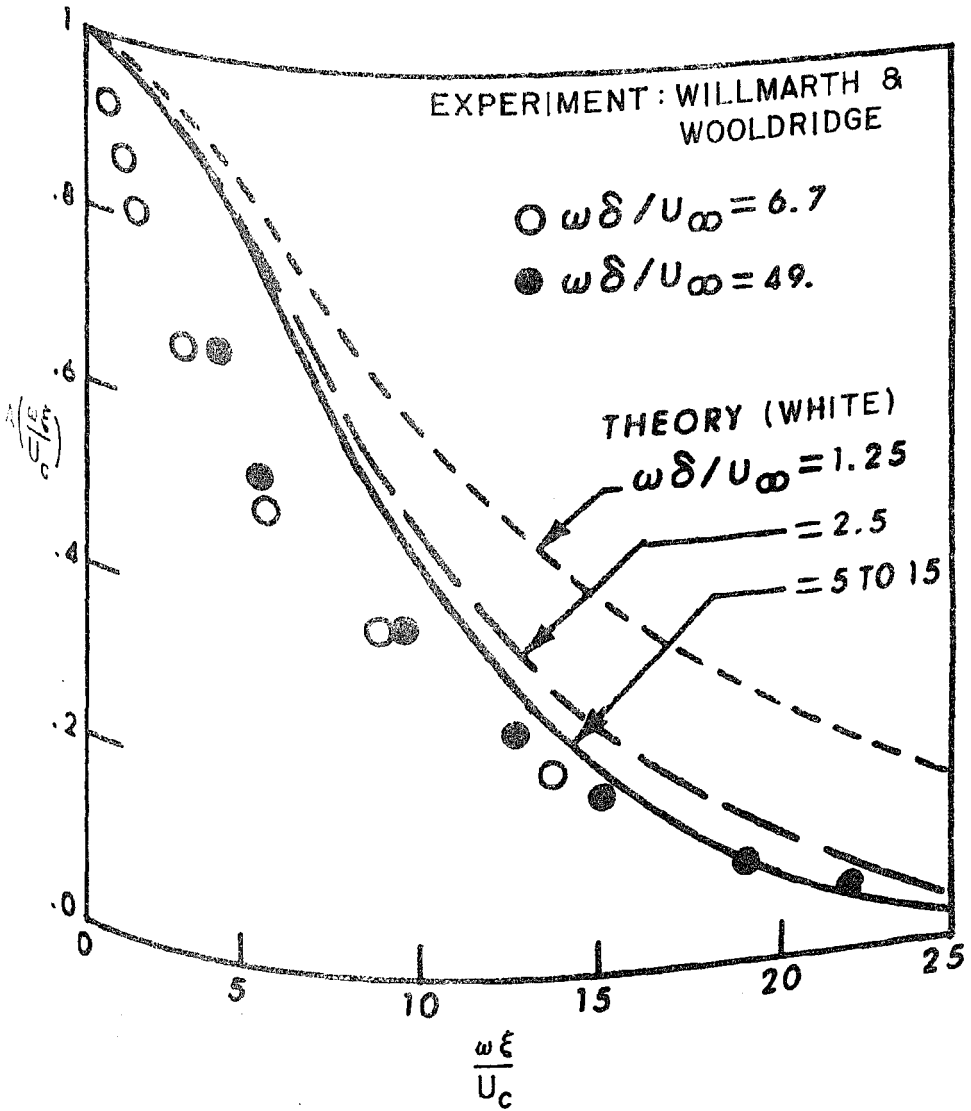
Fig. 5. Optimized longitudinal correlation coefficient (White, 1964, from Fig. 6).
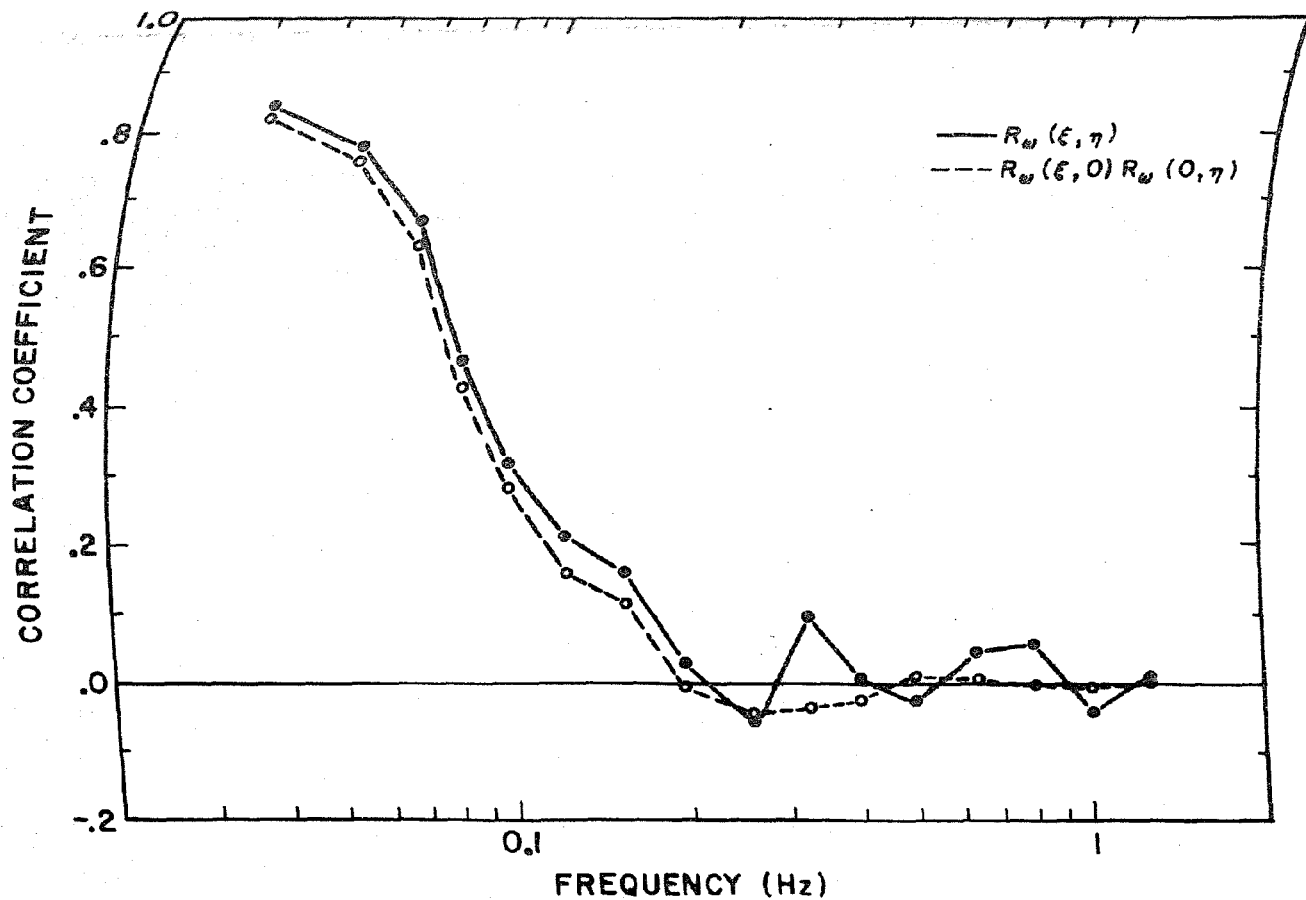
Fig. 6a. A comparison between $R_\omega(\xi,\eta)$ for $\xi = \eta$ and the product $R_\omega(\xi,0)R_\omega(0,\eta)$ for run 08403AB.
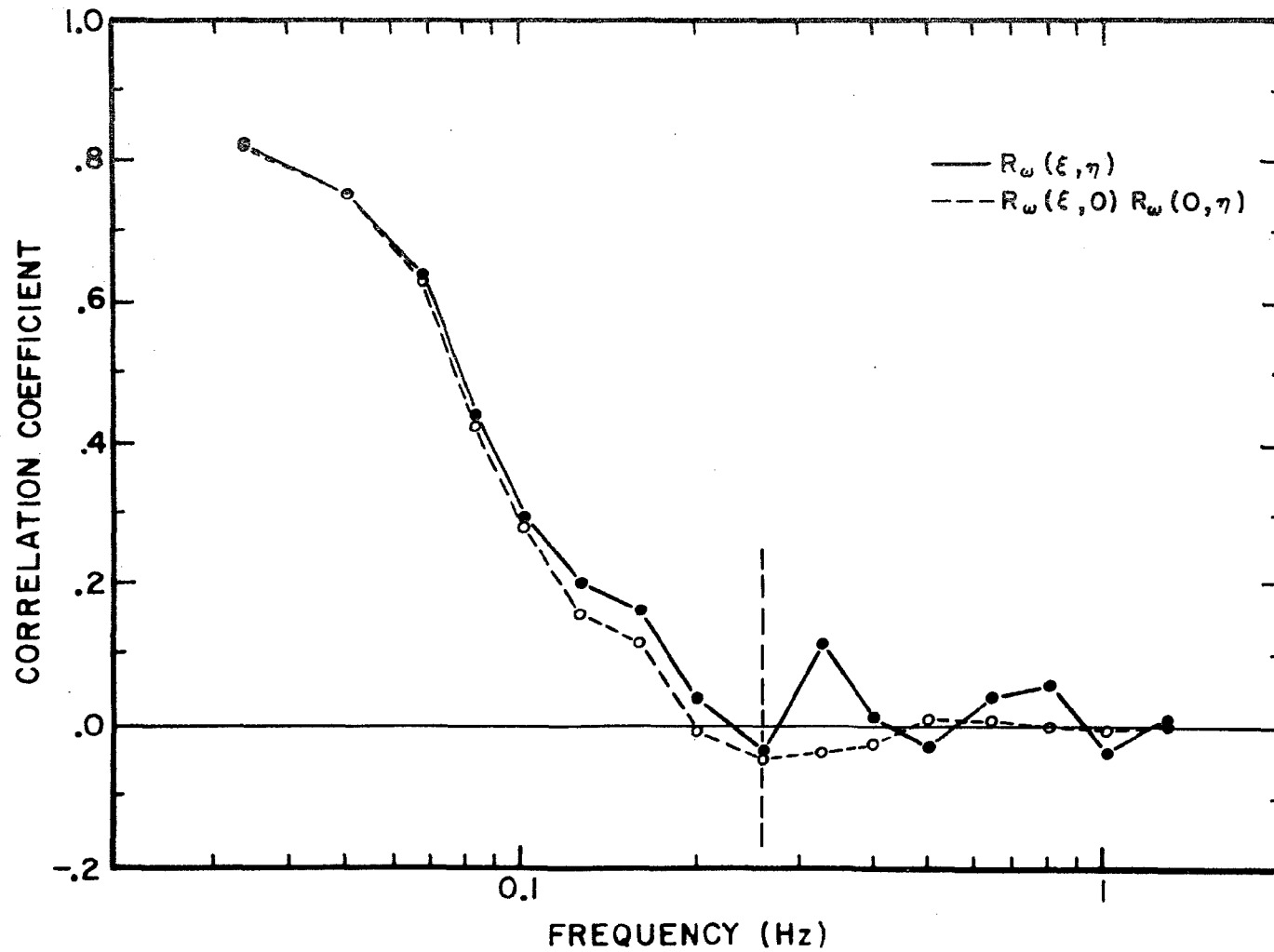
Fig. 6b. A comparison between $R_\omega(\xi,\eta)$ and the product $R_\omega(\xi,0)R_\omega(0,\eta)$ for run 08403AB, corrected for a 7° error in wind direction.
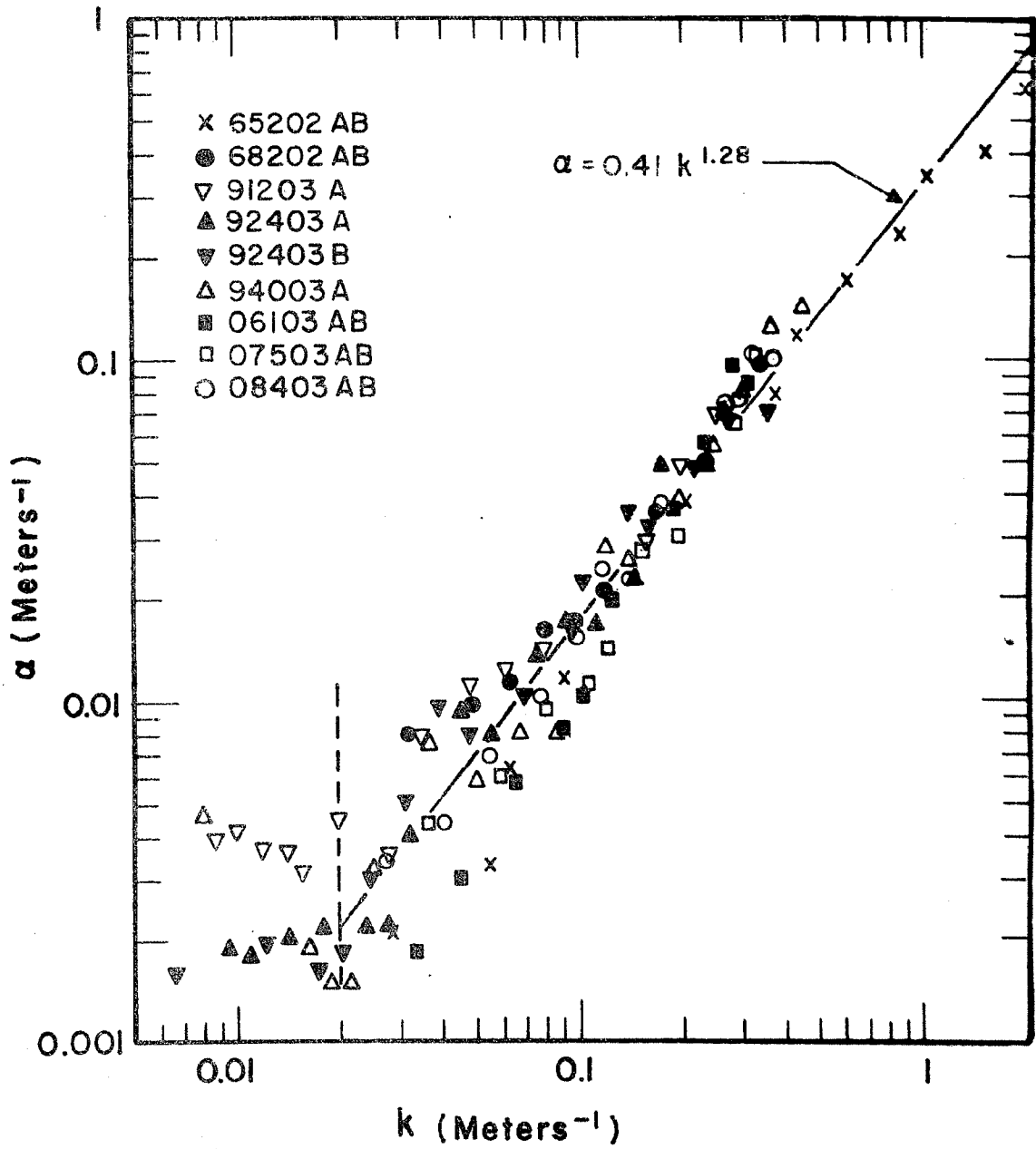
Fig. 7. Reciprocal longitudinal scale α versus wave number k.
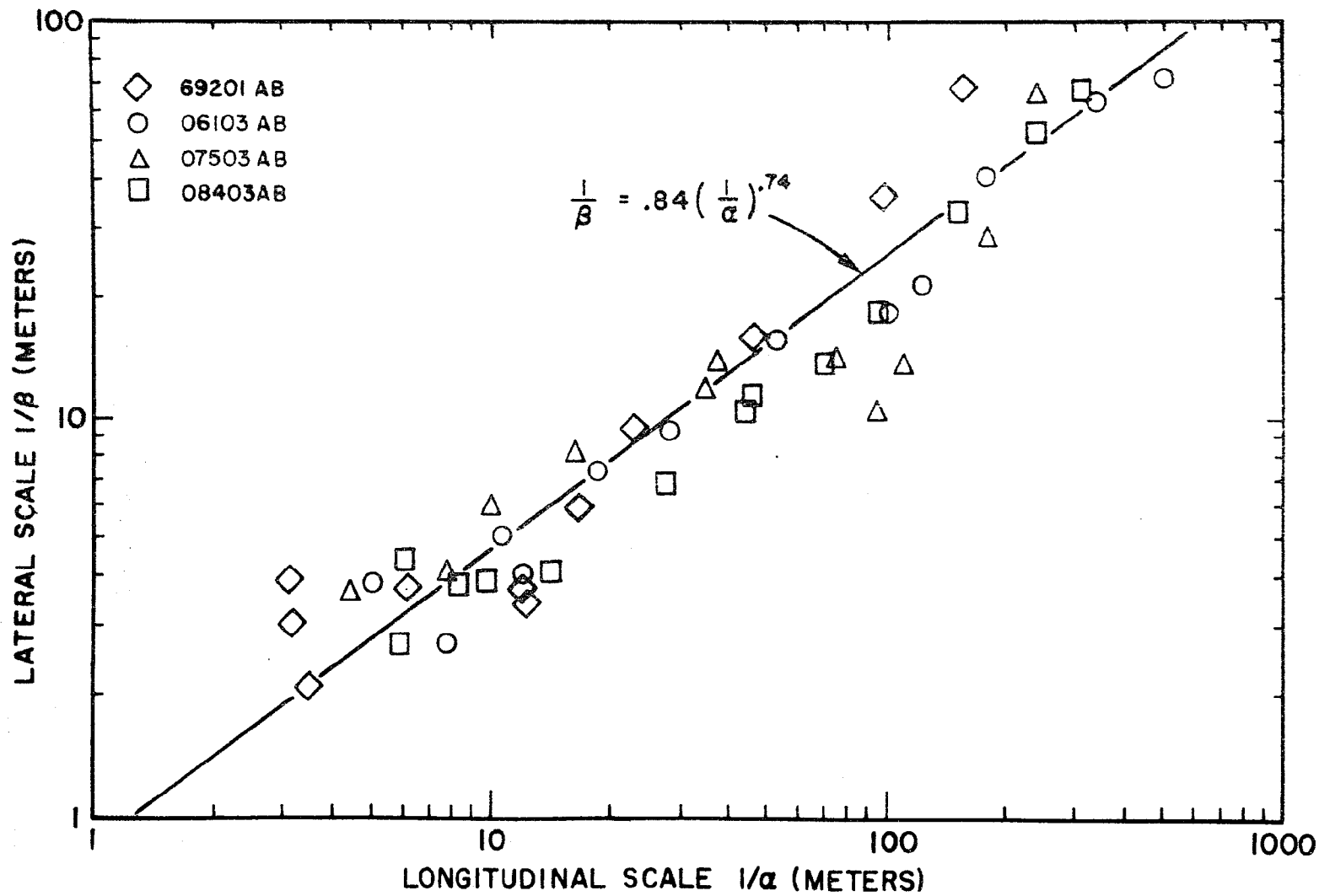
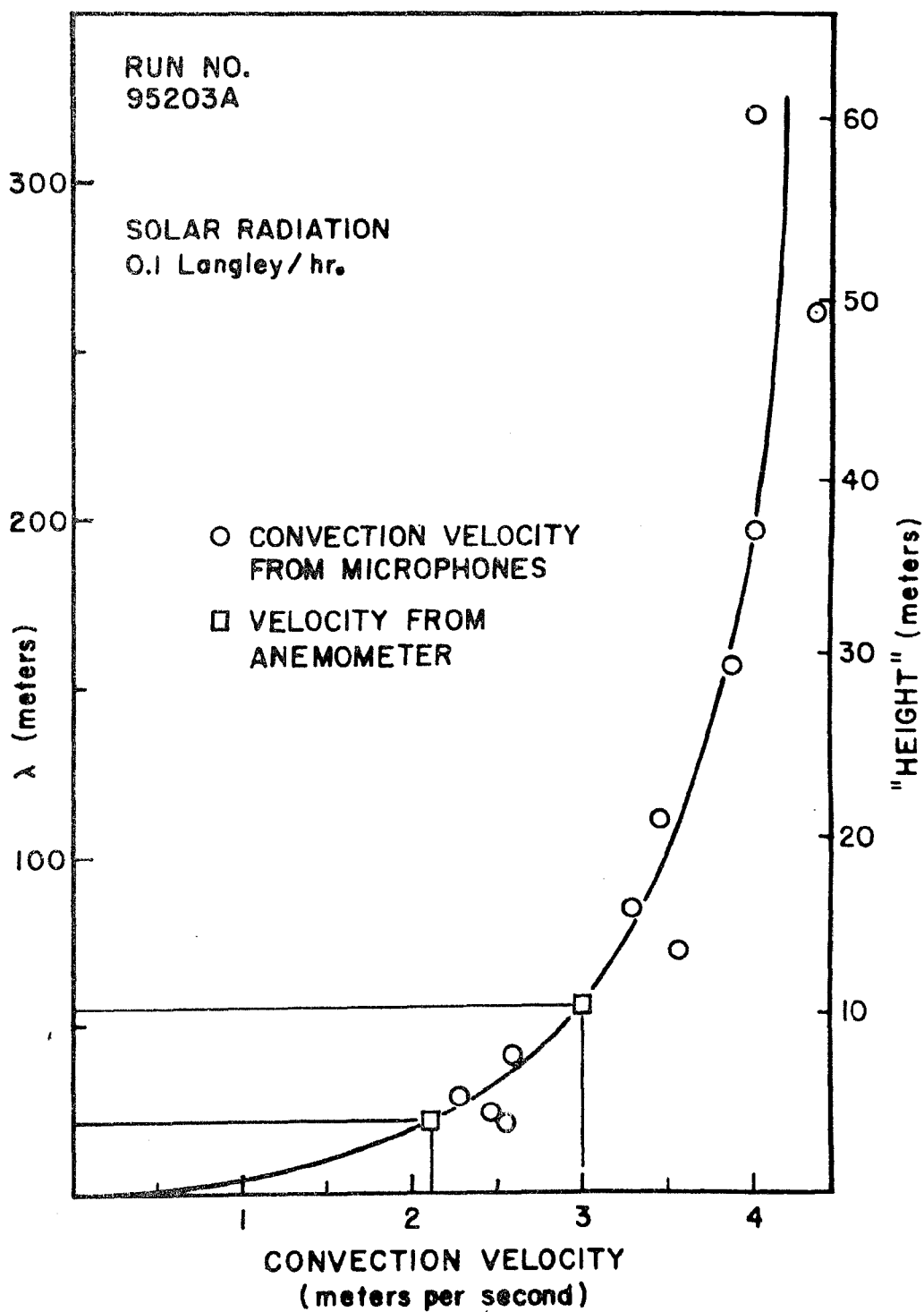Fig. 8.   Lateral scale 1/β versus longitudinal scale 1/α.

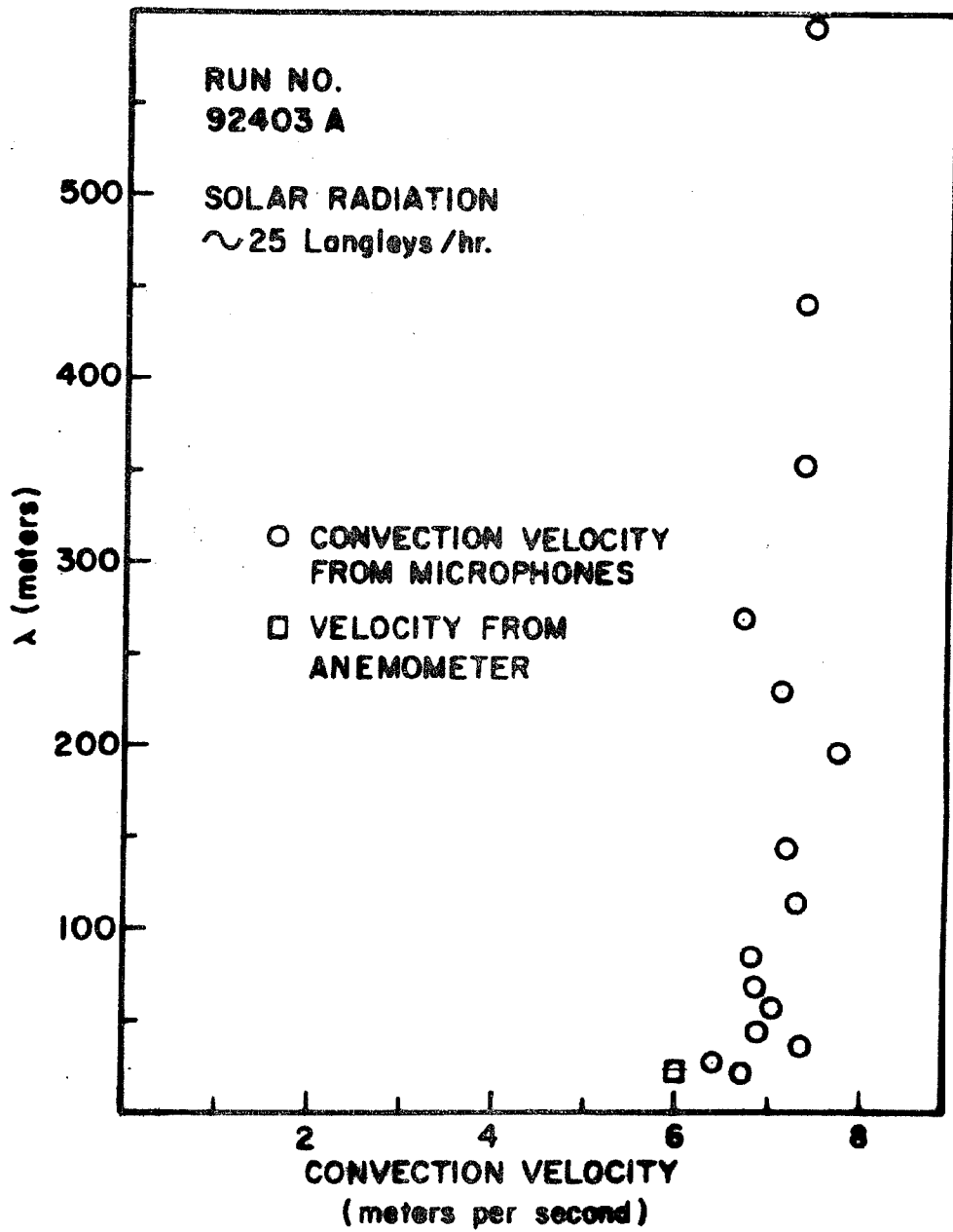Fig. 9   Relation between convection velocity and wavelength for run 92403A.

Fig. 10. Relation between convection velocity and wavelength
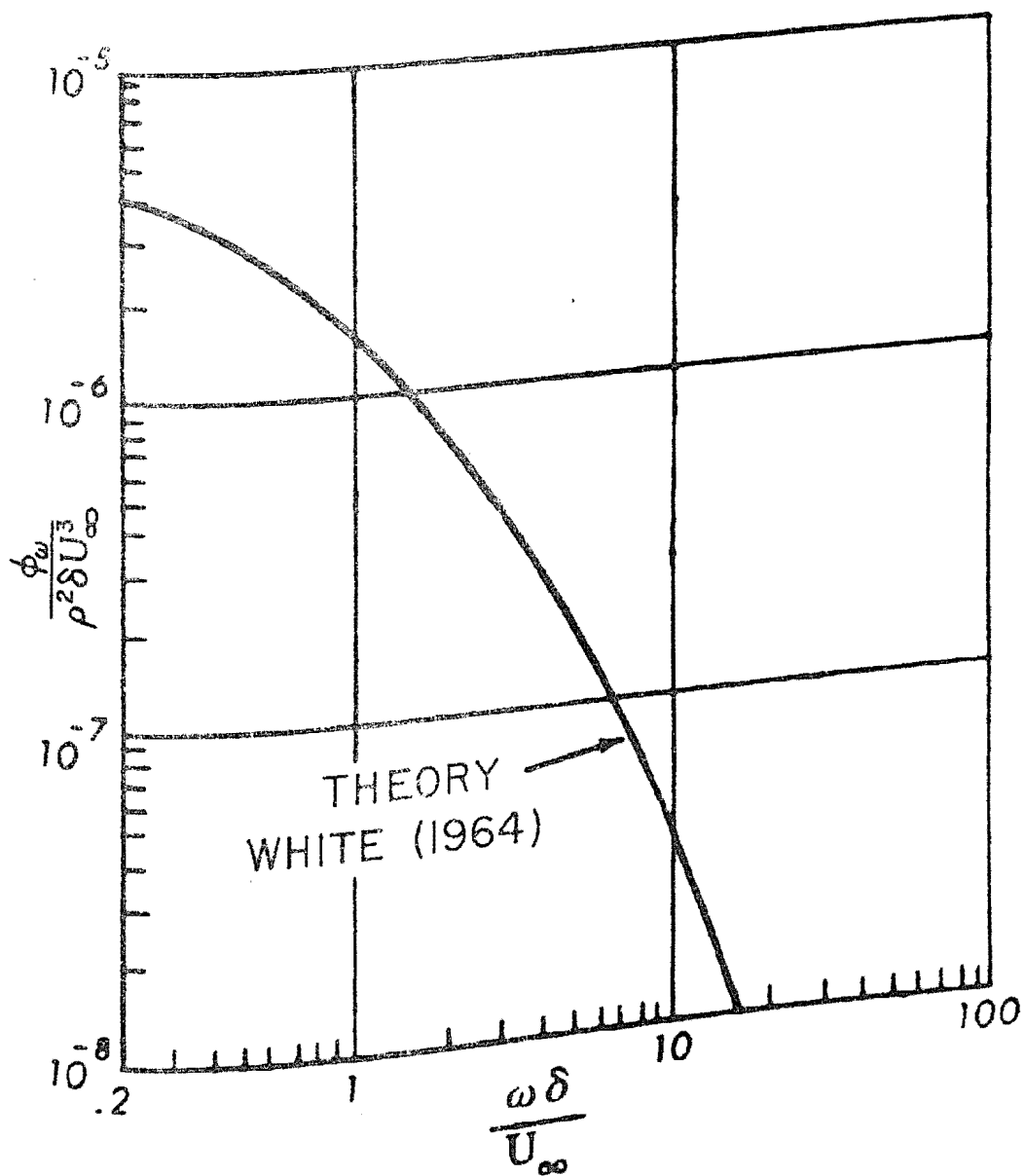for run 92403A.

Fig. 11. The theoretical wall pressure power spectrum of White (1964).
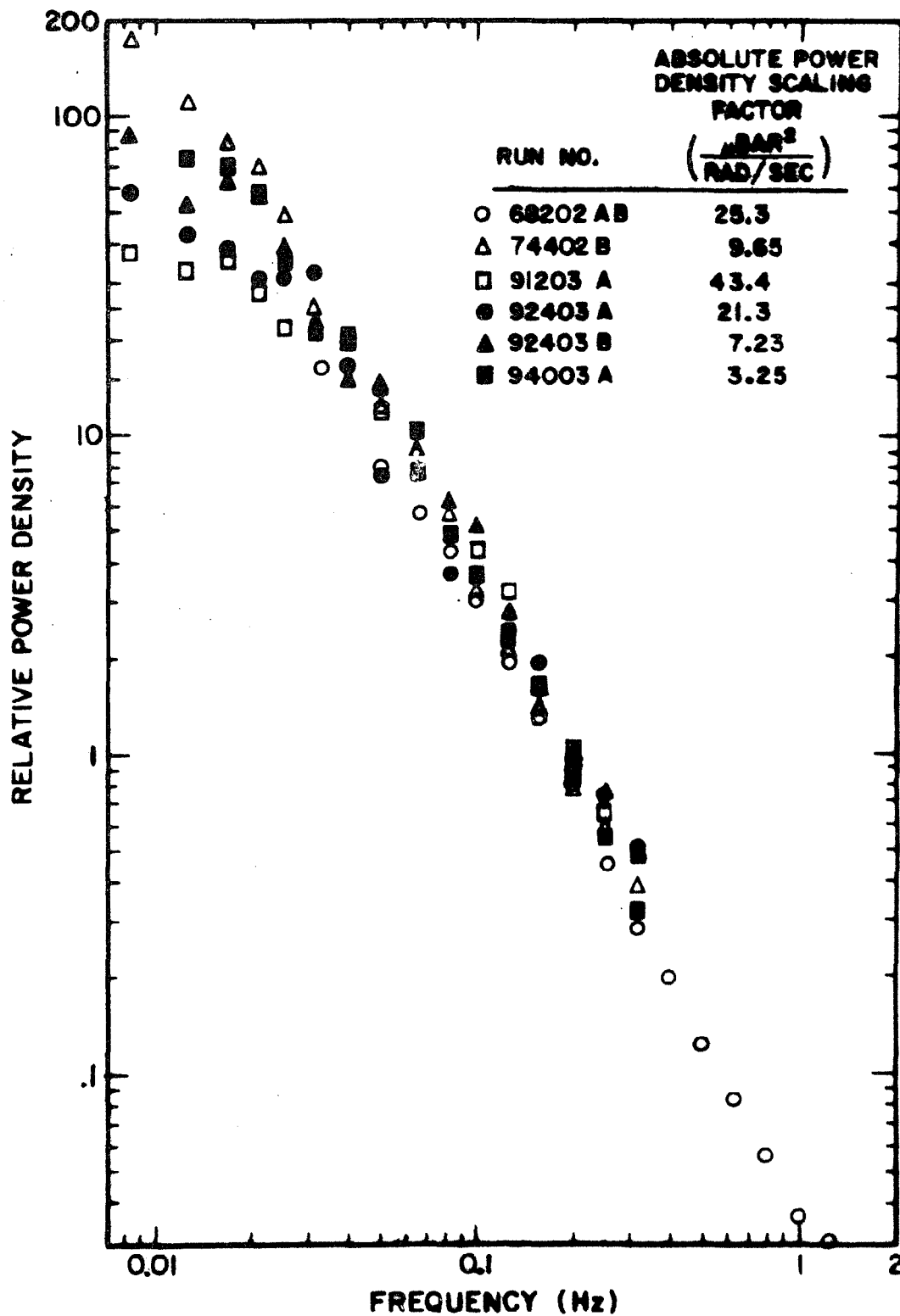
Fig. 12. Composite plot of normalized power spectra for the more typical data.

NOTATION

$A\left(\dfrac{\omega\xi}{U_c}\right)$ Optimized longitudinal correlation coefficient.

$B\left(\dfrac{\omega\eta}{U_c}\right)$ Lateral correlation coefficient.

C_1, C_2, C_3 Acoustical or electrical capacitors.

$Co(\xi,\eta,\omega)$ Co-spectrum.

Coh Coherence.

$Coh^{1/2}(\xi,\eta,\omega)$ Square root of coherence; identical to optimized correlation coefficient.

f Frequency (Hz; i.e., cycles per second).

f_s Sampling rate (samples per second).

$h(t)$ Impulse response function.

k Wave number.

$K(\xi,\eta,\omega)$ Cross-spectral density. Note: $K = Co + iQ$.

$p(x,y,t)$ Fluctuating static pressure on the ground, "wall pressure".

$P(\xi,\eta,\tau)$ Space-time covariance.

$q(x,y,t)$ Narrow-band fluctuating pressure signal.

$Q(\xi,\eta,\omega)$ Quadrature spectrum.

q_A Narrow-band pressure at point A.

q_{BA} That part of the signal q_B which is completely correlated with q_A.

q_{BA*} That part of q_B which is completely uncorrelated with q_A. Note: $q_B = q_{BA} + q_{BA*}$.

R_1, R_2 Accoustical or electrical resistors.

$R_\omega(\xi,\eta)$	Narrow-band correlation coefficient.
$R_\omega^{(m)}(\xi,\eta)$	Correlation coefficient as measured using filters with finite bandwidth.
$R_{opt,\omega}(\xi,\eta)$	Optimized correlation coefficient.
S	Strouhal number.
T_L	Maximum time lag in cross and auto-correlations
U	Average velocity.
U_c	Convection velocity; $U_c = \omega/k$.
U_∞	Free stream velocity.
U_x	Fluctuating velocity in the stream direction.
U_y	Fluctuating component of velocity perpendicular to the stream.
X	Position co-ordinate on the ground in the stream direction.
x(t)	Time varying signal in APPENDIX C.
Y	Frequency response of a filter whose impulse response is h(t).
y	Position co-ordinate on the ground perpendicular to the stream.
y(t)	Time varying signal in APPENDIX C.
α	Longitudinal coherence decay parameter; identical to reciprocal of longitudinal scale.
β	Lateral coherence decay parameter; identical to reciprocal of lateral scale.
γ	Dummy variable in SECTION IV. A constant in APPENDIX C.
Δ	A specified correlation coefficient in SECTION V.
δ	Boundary layer thickness.
$\delta*$	Boundary layer displacement thickness.
ϵ	A number between zero and one.

η	Lateral (perpendicular to stream) component of separation between transducers.
θ	Phase angle of cross-spectral density.
λ	Wavelength.
ξ	Longitudinal (along stream) component of separation between transducers.
τ	Time delay between two signals.
$\phi(\omega)$	"Power" spectral density.
ω	Angular frequency.
μ	Dummy Variable.
ν	Dummy Variable.

APPENDIX B

A BRIEF DESCRIPTION OF THE COMPUTER PROGRAM

USED FOR THE CROSS-SPECTRAL AND POWER SPECTRAL DENSITIES[36]

A. IDENTIFICATION

TITLE: Tukey Spectrum; Cross Spectra and Power Spectra, Fortran

CO-OP ID: G6 UCSD TUKEY

CATEGORY: Time Series Analysis

PROGRAMMER: Gaylord Miller

DATE: August 11, 1961

B. PURPOSE

This is a time series analysis program which contains three basic

subprograms. The first two, filter and removal of trend, prepare

the data (two time series at equal time intervals) for the spectrum

analysis subprogram. Tukey Spectrum computes for the two simultaneous

time series (6,000 or less measurements each) the cross (co-and

quadrature-) spectra and the two power spectra. Phase and coherence

are calculated from the cross-spectra and power spectra. For de-

tailed discussion of the mathematical method, see "The Measurement

of Power Spectra" by Blackman and Tukey, Dover Publications, 1958,

and also the program listing.

C. USAGE

1. This is a main program not a subroutine.

Data deck set-up

---

[36]Copied directly from the description that came with the computer
program.

More than one data deck may be processed in one run.

Each data deck contains up to seven items as follows:

(a) Read control card, Format (11I3)

LOP   -usually "0", this calls a dummy subroutine LOPDEC

which, if used, must be supplied by the user.*

KL   -generates a "1 + cos" set of filter weights KL

time steps long for use as the low-pass filter.

The number of filter weights must be $\leq$ 550.

KH   -generates a "1 + cos" set of filter weights KH

long for use as the high-pass filter. The number

of filter weights must be $\leq$ 50.

NL   -number of filter weights to be read in as a

low-pass filter (KL must be 0 if NL $\neq$ 0).

The number of weights must be $<$ 550.

NH   -number of filter weights to be read in as a

high-pass filter (KH must be 0 if NH $\neq$ 0)

The number of weights must be $<$ 50.

NDCMT   -number of advances for low-pass filter.

Any reasonable number of advances may be used.

NTIMES -number of times low-pass filter is to be

applied. Any reasonable number of times may

be used.

NDEG   -"0" removes mean of series, "1" removes

trend.

INTAPE -input tape number (Fortran number)

---

*LOPDEC, when used, as a subroutine to smooth data, i.e., to low-pass filter and decimate. This permits long series to be spectrum analyzed.

LAGS   -number of spectral estimates and lags in auto- and cross-correlation. Lags must be ≤ 500.

JUBN   -"1" for the last data deck, "0" for pre-ceeding decks.

(b)   Low-pass filter deck, Format (7F10.6)

If NL $\neq$ 0, this filter deck must be present.

(c)   High-pass filter deck, Format (7F10.6)

If NH $\neq$ 0, this filter deck must be present.

(d)   Title Card 1, Format (2A6,I5,F7.1,8A6)

The four items on this card are:

1. Format of the time series data following.

2. Number of elements in the time series, this number must be $\leq 6,000$.

3. Time interval, Δt, for the time series.

4. Title of the series, used only for identification.

(e)   Time series 1, format as specified in (d) and (4) above.

(f)   Title card 2, see item (d) above.

(g)   Time series 2, format as specified in (f) and (4) above.

2. For parameter list see section C.1.

3. 15000 locations are required total.

4. 12000 locations are temporary storage.

5. No alarms or special error printout.

6. No error return.

7. No error stop. A separate test program is used to check the

input data for format and number of samples.**

8. Systems, input and output tapes only.

9. See Section C.1. for format information.

10. There are no jump switch settings.

11. The time required for a data deck is approximately given by:

$$T_{min} = (10^{-5})\text{ (total number of weights in filter + LAGS)}/\text{NDCMT**}$$

(number of elements in series)

12. Single precision, floating point.

13. This program has a dummy subroutine named SAVE; at the points where SAVE is called, the program may be dumped and reloaded at a later time.

14. 1604, Fortran Systems Tape, and an input and output tape.

15. Blackman and Tukey, Dover Publications, 1958.

D. METHOD

See flow diagram and Fortran Listing.

<u>Subroutine Filter</u>

This subroutine performs a simple running weighted average. The weights W_k are either supplied by the user or if KH or KL $\neq$ 0, are generated by the main program.

$$X_i = \sum_{k=0}^{n-1} B_{i+k} W_k$$

In the above:

B_i is the original series.

X_i is the filtered series.

**As a single bad number in the midst of the data will drastically change the spectrum it is often advisable to check first differences for reasonableness in addition to checking the input data for correctness of form.

W_k is the weighting function.

The filtered series is always shorter than the original series by the number of weights n, minus one.

If NDCMT $\neq$ 1 then X_i is computed only for i = 1, 1+NDCMT, 1+2xNDCMT, 1+3x NDCMT, ...

Subroutine Datrend

This subroutine removes the mean from a time series and if NDEG = 1 removes the "least squares trend".

Subroutine Coquad

This subroutine computes the auto- and cross-correlations and from these, the spectra and cross-spectra.

$$A(\ell) = \frac{1}{n-1} \sum_{i=\ell+1}^{n} X_{i-\ell} X_i - \frac{1}{(n-1)^2} \sum_{i=\ell+1}^{n} X_{i-\ell} \sum_{i=\ell+1}^{n} X_i$$

$$B(\ell) = \frac{1}{n-1} \sum_{i=\ell+1}^{n} Y_{i-\ell} Y_i - \frac{1}{(n-1)^2} \sum_{i=\ell+1}^{n} Y_{i-\ell} \sum_{i=\ell+1}^{n} Y_i$$

$$C(\ell) = \frac{1}{n-1} \sum_{i=\ell+1}^{n} X_{i-\ell} Y_i - \frac{1}{(n-1)^2} \sum_{i=\ell+1}^{n} X_{i-\ell} \sum_{i=\ell+1}^{n} Y_i$$

$$D(\ell) = \frac{1}{n-1} \sum_{i=\ell+1}^{n} Y_{i-\ell} X_i - \frac{1}{(n-1)^2} \sum_{i=\ell+1}^{n} Y_{i-\ell} \sum_{i=\ell+1}^{n} X_i$$

$A(\ell)$, $B(\ell)$, $C(\ell)$ and $D(\ell)$ are the auto and cross correlations of the time series X_i and Y_i; ℓ is the lag and equals 0,1,2....up to a maximum lag m; n is the maximum value of the subscript i. The second term in each of the above expressions simply allows for the changes in the means of X_i and Y_i as ℓ varies (those parts of the lagged series that do not overlap are dropped).

$$E(\ell) = \frac{D(\ell) + C(\ell)}{2}$$

$$F(\ell) = \frac{D(\ell) - C(\ell)}{2}$$

$E(\ell)$ is the even part of the cross-correlation; $F(\ell)$ is the odd part of the cross-correlation.

$$x(k) = \frac{\delta_k}{m} \left[\sum_{\ell=1}^{m-1} 2\epsilon(\ell) \cos \frac{k\ell\pi}{m} A(\ell) + A(0) \right]$$

$$y(k) = \frac{\delta_k}{m} \left[\sum_{\ell=1}^{m-1} 2\epsilon(\ell) \cos \frac{k\ell\pi}{m} B(\ell) + B(o) \right]$$

$$z(k) = \frac{\delta_k}{m} \left[\sum_{\ell=1}^{m-1} 2\epsilon(\ell) \cos \frac{k\ell\pi}{m} E(\ell) + E(0) \right]$$

$$w(k) = \frac{\delta_k}{m} \left[\sum_{\ell=1}^{m-1} 2\epsilon(\ell) \sin \frac{k\ell\pi}{m} F(\ell) + F(0) \right]$$

where $\delta_k = \frac{1}{2}$ for $K = 0$ or m

$\delta_k = 1$ otherwise

$2\epsilon(\ell) = 1 + \cos \frac{\pi\ell}{m}$

$x(k)$ and $y(k)$ are the spectra of X_i and Y_i. $z(k)$ and $w(k)$ are the co- and quadrature-spectra. k is the dimensionless frequency.

Two other often useful quantities are calculated: $R^2(k)$ the coherence squared and $\phi(k)$ the phase lead of Y_i over X_i.

$$R^2(k) = \frac{w^2(k) + z^2(k)}{x(k)y(k)}$$

$$\phi(k) = \text{ARCTAN} \frac{w(k)}{z(k)}$$

APPENDIX C

A THEOREM RELATING TO CORRELATION OF SIGNALS

Given: Let $x(t)$ and $y(t)$ be two signals and let R_{xy} be the correlation coefficient between them.

To Prove: Show that $y(t)$ may be divided into two parts, viz.

$y = y_1 + y_2$, such that y_1 is completely correlated with x

and y_2 is completely uncorrelated with x; i.e., $R_{xy_1} = 1$

and $R_{xy_2} = 0$.

The first requirement is fulfilled if $y_1 = \Upsilon x$ where Υ is any constant.

$$R_{xy_1} = \frac{\overline{xy_1}}{\sqrt{\overline{x^2}\,\overline{y_1^2}}} = \frac{\overline{x\Upsilon x}}{\sqrt{\overline{x^2}\,\Upsilon^2\,\overline{x^2}}} = \frac{\Upsilon\,\overline{x^2}}{\Upsilon\,\overline{x^2}} = 1 \tag{C1}$$

Therefore,

$$y = \Upsilon x + y_2 \text{ or } y_2 = y - \Upsilon x. \tag{C2}$$

To enforce the second condition we require,

$$R_{xy_2} = \frac{\overline{xy_2}}{\sqrt{\overline{x^2}\,\overline{y_2^2}}} = 0 \tag{C3}$$

from which

$$\overline{xy_2} = 0$$

$$\overline{x(y-\Upsilon x)} = 0$$

$$\overline{xy} - \overline{x^2\Upsilon} = 0.$$

Therefore we have

$$\Upsilon = \frac{\overline{xy}}{\overline{x^2}}. \tag{C4}$$

Let us compute Υ in terms of R_{xy} and the rms values of the signals x and y.

$$\gamma = \frac{\overline{xy}}{\overline{x^2}}$$

$$\gamma = R_{xy}\frac{\overline{xy}}{\overline{x^2}}\frac{1}{R_{xy}}$$

$$\gamma = R_{xy}\frac{\overline{xy}}{\overline{x^2}}\frac{\sqrt{\overline{x^2}}\sqrt{\overline{y^2}}}{\overline{xy}}$$

Therefore we have the result,

$$\gamma = \frac{\sqrt{\overline{y^2}}}{\sqrt{\overline{x^2}}}R_{xy} \qquad (C5)$$

from which the correlated part of the signal is

$$y_1 = \frac{\sqrt{\overline{y^2}}}{\sqrt{\overline{x^2}}}R_{xy}x_o \qquad (C6)$$

REFERENCES

Bakewell, Henry P., Jr., Carey, George F., Libuha, John J., Schloemer,
    Howard H., and Von Winkle, William A. (1962) Wall Pressure
    Correlations in Turbulent Pipe Flow. U. S. Navy Underwater
    Sound Laboratory Report, no. 559.

Bakewell, Henry P., Jr. (1963) Longitudinal Space-Time Correlation
    Function in Turbulent Airflow. J. Acoust. Soc. Am. Vol. 35,
    no. 6, 936-937.

Bakewell, Henry P., Jr. (1964) Narrow-Band Investigations of the
    Longitudinal Space-Time Correlation Function in Turbulent Airflow.
    J. Acoust. Soc. Am., Vol. 36, no. 1, 146-148.

Bull, M. K. (1963) Space Time Correlations of the Boundary Layer
    Pressure Field in Narrow Frequency Bands. University of Southamp-
    ton A.A.S.U. Report, no. 200.

Bull, M. K., Wilby, J. F., Blackman, D. R. (1963) Wall Pressure
    Fluctuations in Boundary Layer Flow and Response of Simple
    Structures to Random Pressure Fields. University of Southampton
    A.A.S.U. Report, no. 243.

Cook, R. K. (1962) Strange Sounds in the Atmosphere, Part I. Sound,
    Vol. 1, no. 2, 12-16.

Cook, R. K., and Young, Jessie M. (1962) Strange Sounds in the
    Atmosphere, Part II. Sound, Vol. 1, no. 3, 25-33.

Corcos, G. M. (1962) Pressure Fluctuations in Shear Flows. Univer-
    sity of California Institute of Engineering Research Report,
    Series 183, no. 2.

Corcos, G. M. (1963) Resolution of Pressure in Turbulence. J. Acoust.
    Soc. Am., Vol. 35, no. 2, 192-199.

Corcos, G. M. (1964) The Structure of the Turbulent Pressure Field
    in Boundary-Layer Flows. J. Fluid Mech., Vol. 18, 353-378.

Daniels, Fred B. (1959) Noise-Reducing Line Microphone for Frequencies
    Below 1 Hz. J. Acoust. Soc. Am., Vol. 31, no. 4, 529-531.

Dryden, Hugh L., Schubauer, G. B., Mock, W. C., Jr., and Skramstad,
    H. K. (1937) Measurements of Intensity and Scale of Wind-Tunnel
    Turbulence and Their Relation to the Critical Reynolds Number
    of Spheres. National Advisory Committee for Aeronautics Report,
    no. 581.

Dyer, Ira. (1958) Sound Radiation Into a Closed Space From Boundary Layer Turbulence. Bolt, Beranek, and Newman, Inc., Report, no. 602.

Gardner, Sheldon. (1963) Surface Pressure Fluctuations Produced By Boundary Layer Turbulence. Office of Naval Research, Technical Research Group, 142-TN-63-5.

Gossard, Earl E. (1960) Spectra of Atmospheric Scalars. J. Geophys. Res., Vol. 65, no. 10, 3339-3351.

Harrison, Mark. (1958) Pressure Fluctuations on the Wall Adjacent To a Turbulent Boundary Layer. David Taylor Model Basin Report, no. 1260.

Hinze, J. O. (1959) Turbulence. New York: McGraw-Hill Book Co., Inc.

Kraichnan, R. H. (1956a) Pressure Field Within Homogeneous Anisotropic Turbulence. J. Acoust. Soc. Am., Vol. 28, no. 1, 64-72.

Kraichnan, R. H. (1956b) Pressure Fluctuations in Turbulent Flow Over a Flat Plate. J. Acoust. Soc. Am., Vol. 28, no. 3, 378-390.

Lilley, G. M., and Hodgson, T. H. (1960) On Surface Pressure Fluctuations in Turbulent Boundary Layers. AGARD Report, no. 276.

Lilley, G. M. (1963) Wall Pressure Fluctuations Under Turbulent Boundary Layers At Subsonic and Supersonic Speeds. AGARD Report, no. 454.

Lin, C. C. (1952) On Taylor's Hypothesis and the Acceleration Terms In the Navier-Stokes Equations. Quarterly App. Maths., Vol. 10, 295-306.

Lumley, John L., and Panofsky, Hans A. (1964) The Structure of Atmospheric Turbulence. New York: Interscience Publishers.

MacCready, Paul B., Jr. (1962) The Inertial Subrange of Atmospheric Turbulence. J. Geophys. Res., Vol. 67, no. 3, 1051-1059.

Richie, W. C. (1956) Report on Research to Investigate Atmospheric Intrasonic Pressure Variations. University of Texas Defense Research Laboratory Report, DRL-A 237.

Serafini, John (1962) Wall-Pressure Fluctuations In a Turbulent Boundary Layer. California Institute of Technology, Ph.D. Thesis.

Serafini, John S. (1963) Wall-Pressure Fluctuations and Pressure-Velocity Correlations In Turbulent Boundary Layers. AGARD Report, no. 453.

Skudrzyk, E. J., and Haddle, G. P. (1960) Noise Production In a Turbulent Boundary Layer By Smooth and Rough Surfaces. J. Acoust. Soc. Am., Vol. 32, no. 1, 19-34

Taylor, G. I. (1922) Diffusion By Continuous Movements. Proc. London Math. Soc. Second Series, Vol. 20, 196-212.

White, Frank M. (1964) A Unified Theory of Turbulent Wall Fluctuations. U. S. Navy Underwater Sound Laboratory Report, no. 629.

Willmarth, W. W. (1959) Space-Time Correlations and Spectra of Wall Pressure In a Turbulent Boundary Layer. NASA Technical Memorandum, no. 3-17-59W.

Willmarth, W. W., and Wooldridge, C. F. (1962) Measurement of the Fluctuating Pressure At the Wall Beneath a Thick Turbulent Boundary Layer. J. Fluid Mech., Vol. 14, 187-210.

Wills, J. A. B. (1963) On Convection Velocities In Turbulent Shear Flows. AGARD Report, no. 457.

VITA

Name: Joseph Tant Priestley.

Permanent address: 3412 Highview Ct., Silver Spring, Maryland 20902.

Degree and date to be conferred: M.S., 1965.

Date of birth: Memphis, Tennessee.

Secondary education: David Lipscomb High School, 1953.

Collegiate institutions attended	Dates	Degree	Date of Degree
David Lipscomb College	1953-55		
Georgia Institute of Technology	1955-57	B.S.	1958
University of Maryland	1959-65	M.S.	1965

Major: Physics.

Minor: Mathematics.

Position held: Physicist, National Bureau of Standards, Washington,

D. C. 20234.